NARI
NASA AERONAUTICS RESEARCH INSTITUTE

Flexible Micropost Arrays for Shear Stress Measurement

Christopher Wohl, Frank Palmieri, Yi Lin, John Connell
NASA Langley Research Center, Advanced Materials and Processing Branch

Xiaoning Jiang, Ashok Gopalarathnam, Yong Zhu, Aditya Saini, Jinwook Kim, Taeyang Kim, Zheng Cui
North Carolina State University, Department of Mechanical and Aerospace Engineering

NASA Aeronautics Research Mission Directorate (ARMD)
2015 Seedling Phase II Technical Seminar
November 17 & 19, 2015

c.j.wohl@nasa.gov, frank.l.palmieri@nasa.gov

The Research Team

NASA LaRC-Materials

Chris Wohl

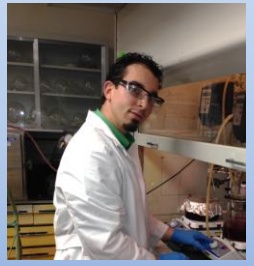

Polymer Physics

Frank Palmieri

Microfabrication

Yi Lin

Nanomaterials

John Connell

Polymeric Materials

NCSU-Fluid Dynamics

Ashok Gopalarathnam

Fluid Physics

Xiaoning Jiang

Microfabrication

Yong Zhu

Nanotechnology

Aditya Saini

Microfence

Taeyang Kim

Piezoelectric

Zheng Cui

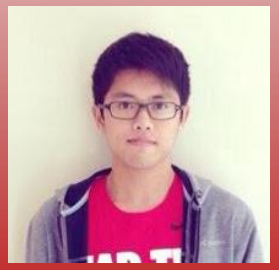

Capacitance

Sensor Type

Why Measure Shear Stress?

- Useful for:
  - Reducing drag in aircraft design
  - Noise abatement
  - Fuel/air mixing
  - …

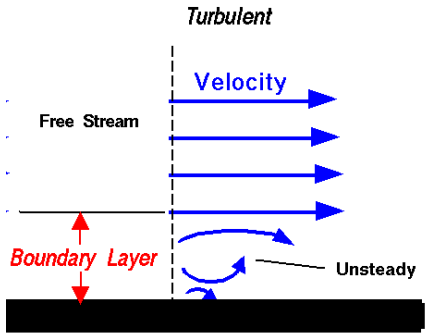

Academic

LaRC Shear Flow Wind Tunnel (20” x 28”)

Practical

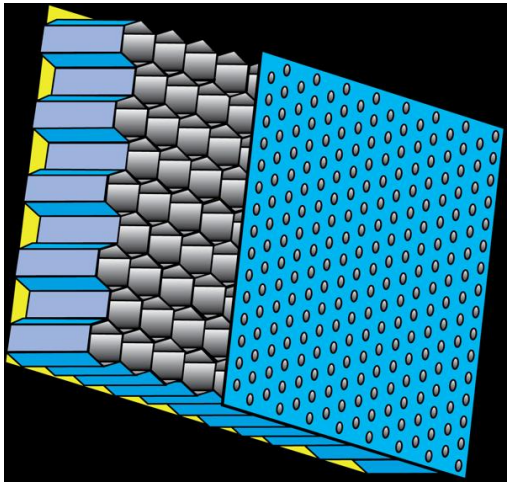

Gerhold & Jones, NARI Phase II Seedling presentation, March 18-19, 2015

Where is Shear Stress Measured?

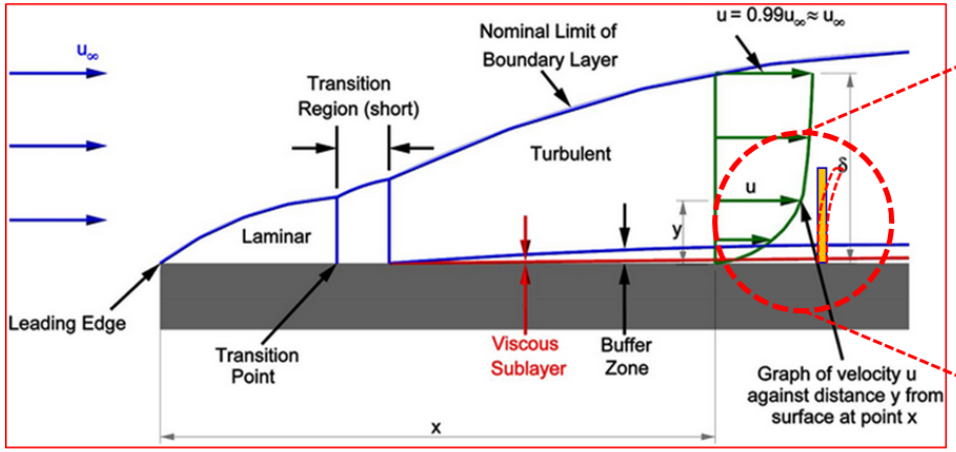

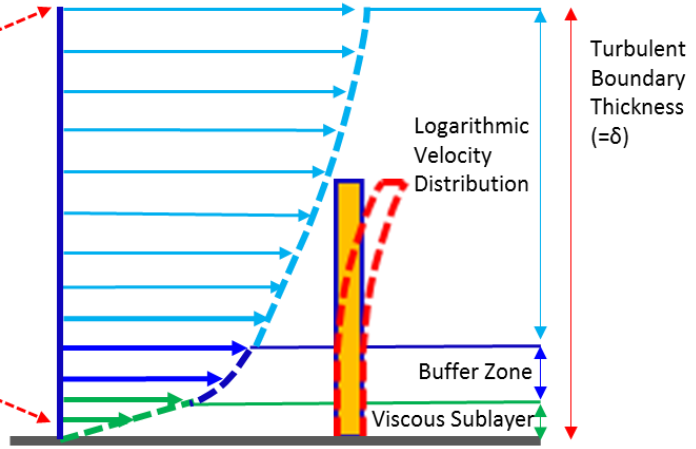

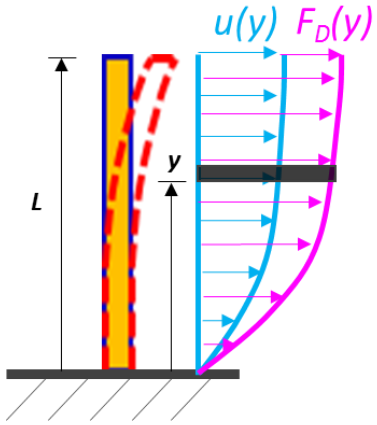

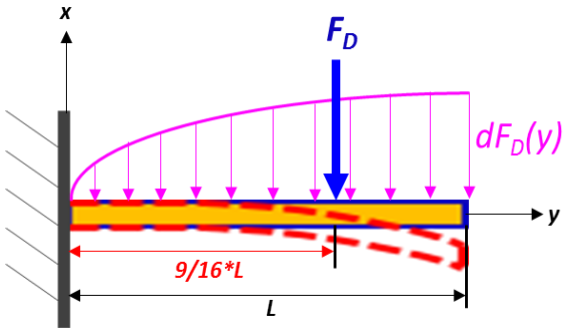

Profile Drag

Mechanical Force

How is Shear Stress Measured?

- Natural Systems
  - Nature's fliers and swimmers possess integrated sensory receptors that are adapted efficiently to detect any disturbing phenomenon during flight, as early as possible, and provide necessary feedback for control

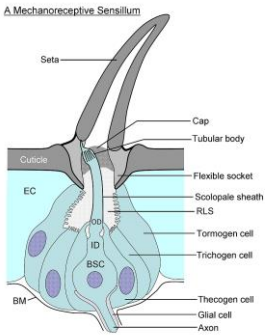

Insect's trichoid sensillum
http://cronodon.com/BioTech/insect_mechanoreceptors.html

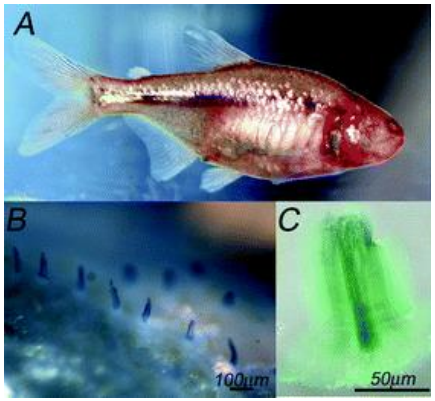

Soft Matter, 2009, 5, 292.

How is Shear Stress Measured?

- Indirect approaches
  - Hot-wire, heat flux gages, oil interferometry, laser Doppler anemometry, fences
- Direct approaches
  - Whispering gallery mode devices, floating recessed components (MEMS)

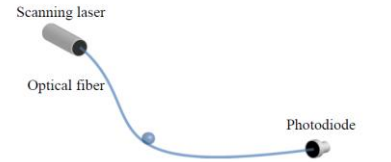

Figure 1: Schematic representation of WGM sensor

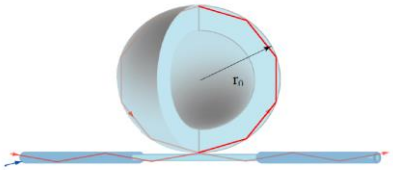

Figure 2: Optical path in the fiber and a coupled hollow microsphere

Whispering Gallery Mode Sensor

44th AIAA Aerospace Sciences Meeting, Paper 649, Reno, NV, Jan. 9-12, 2006

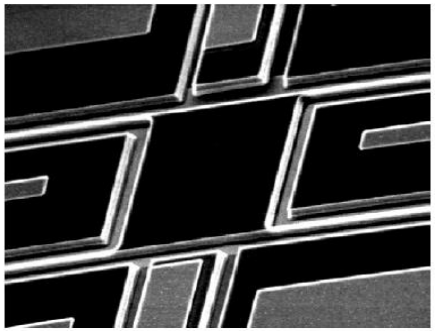

Fig. 2. A scanning electron micrograph (SEM) of a 120 μm × 120 μm × 7 μm floating-element sensor.

MEMS Sensor

Progress in Aerospace Sci., 2002, 38, 515.

Why a New Shear Stress Sensor?

- Implementation difficulty
- Potential airflow disruption
- Sensor complexity
- Fabrication cost
- Sensitivity to contamination

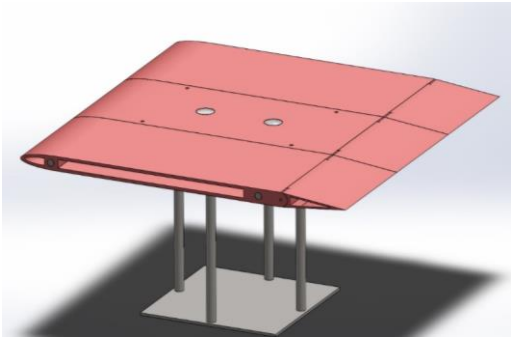

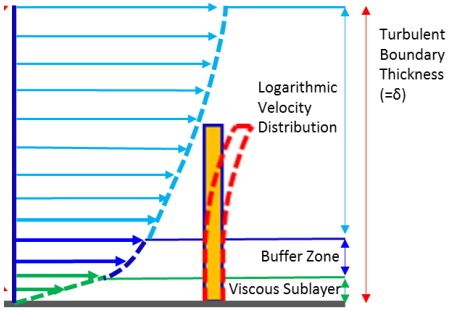

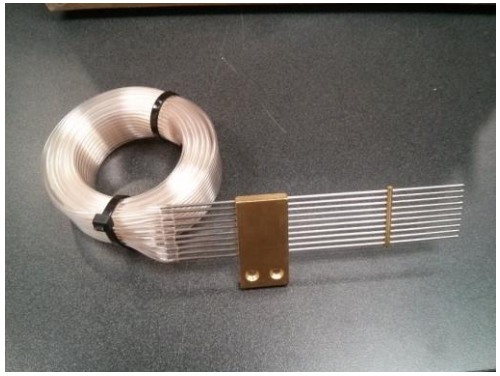

NIST Center for Nanoscale Science and Technology

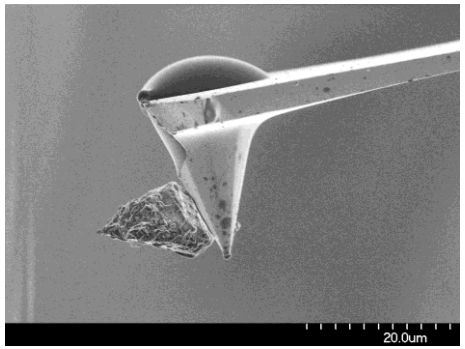

Shear Stress Sensing via Micrometer-Sized Features

The velocity profile in a Turbulent boundary layer

$$\tau_w = \mu \frac{\partial U}{\partial y}\bigg|_{y=0}$$

Dimensionless quantities:
Indicated by $^+$

$$y^+ = \frac{yu^*}{\nu} \qquad U^+ = \frac{U}{u^*}$$

$$\delta^+ = \frac{\delta u^*}{\nu}$$

- y is the distance from the wall made dimensionless with friction velocity, u^*, and kinematic viscosity, ν
- δ is the distance to the free stream velocity, U_e

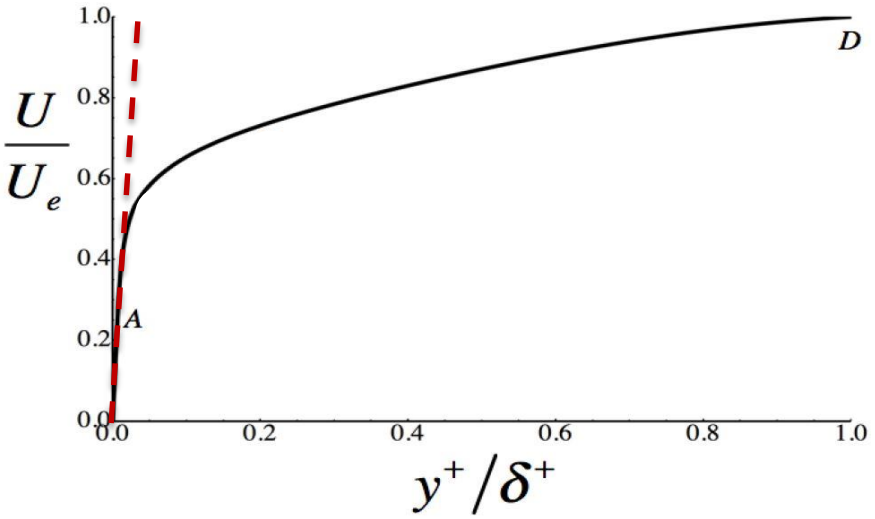

Viscous sublayer – (for $y+ < 5$)
In this region, the velocity profile can be assumed as linear. For above graph, δ^+ is approximately 100.

The viscous sublayer will be approximately 100 μm for typical low speed wind tunnel laboratory flows.

Micropillar Research-Very Complex

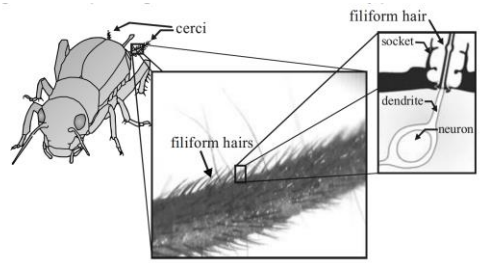

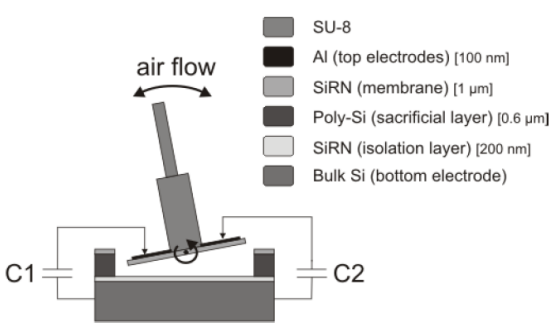

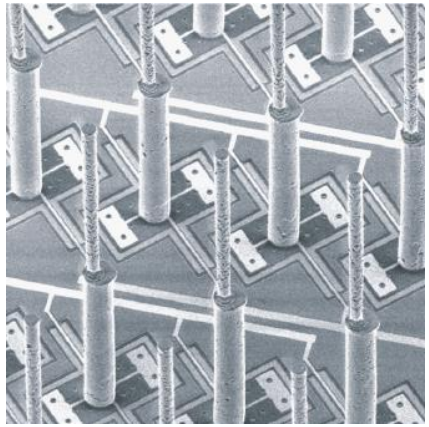

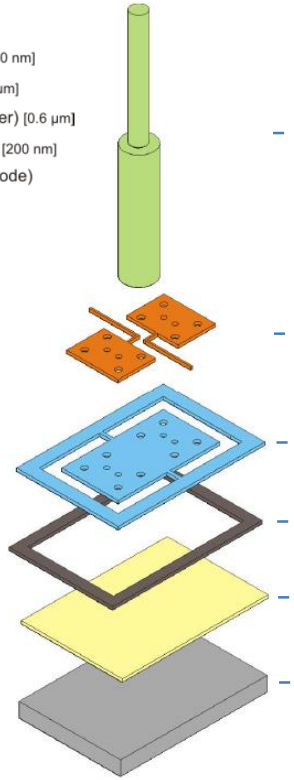

Mechanism:

Hair deflection ➔ Gap change ➔ Capacitance Change ➔ Angle Tilted ➔ Flow rate

Fabrication of SU-8 Hair:

UV Photolithography

Dimension:

Diameter: 50 μm (bottom)/ 25 μm(top)

Height: 2 × 450 μm

Jaganathara, R. K. et. Al., IEEE, 2009

Micropillar Research-Simpler

- Brücker, Große, and Schröder have studied micropillars extensively, but have only demonstrated deflection in liquid flows

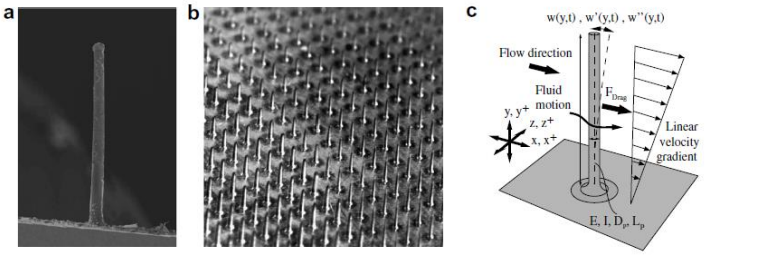

Fig. 1. (a) Scanning electron microscope image of a single pillar and (b) image of a pillar array. (c) Mechanical model of the pillar sensor.

Int. J. Heat Fluid Flow 2008, 29, 830

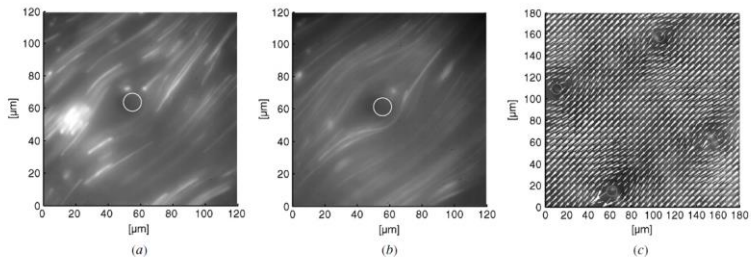

Figure 1. Streaklines of the flow around a pillar indicated by the white circles at 67 rpm (*a*) and 200 rpm (*b*). (*c*) Result from μPIV measurement of the flow around pillars at 40 rpm. Optical focus 25 μm in the fluid. Local Reynolds number based on pillar diameter 5.26×10^{-4}. The measurements were performed using paraffin.

Meas. Sci. Technol. 2006, 17, 2689

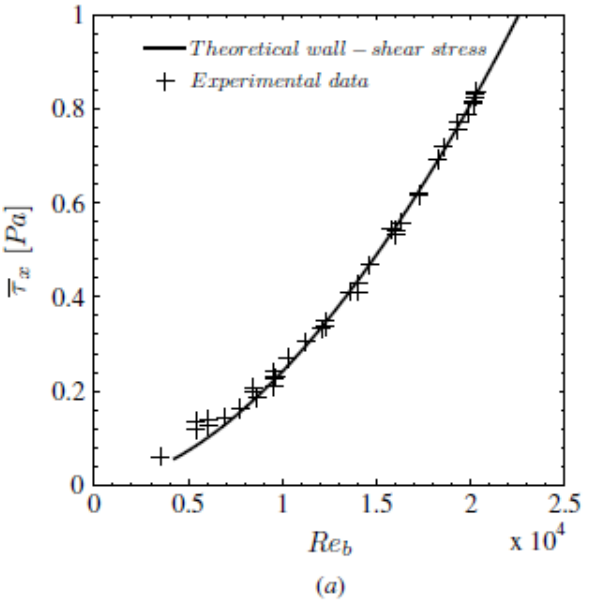

Meas. Sci. Technol. 2008, 19, 015403

Our Approach
S^3 via Elastic Microfence Structures

- Advantages:
  - Robustness
  - Ease of replication
  - Low cost compared to other methods
  - Use of optical detection eliminates the need for any secondary support at the sensor location
  - Detect two-dimensional wall shear stress
  - Micro-size allows for higher spatial resolution

Elastic Microfence Design

- Size

  Force P = profile drag

  $D = \rho v^2 c_D S/2$

  S=LW

  Euler-Bernoulli Theory for Cantilever beam:

  $$\gamma = \frac{PL^3}{3EI} \quad (\delta << L)$$

  L= 50-100 μm (submerged in viscous sublayer)

- Material: silicone rubber
  - Robust, stable over broad temperature range
  - Chemically inert
  - Commercially available
  - Can be dyed

Feature Layout

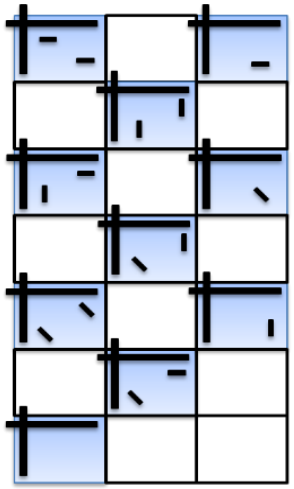

3 x 6 sensor array

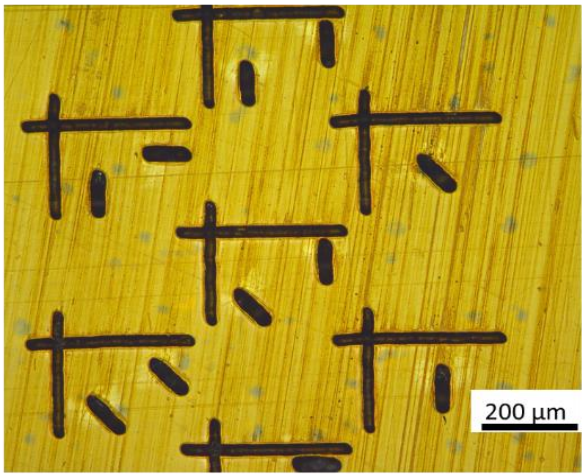

Laser ablation patterned Kapton® HN

Dimensions of individual sensor “die” dictated by field-of-view of the microscope: 0.64 mm X 0.48 mm

Microfence Template Generation

- Direct-write templates by laser-ablating an epoxy plaques
- Frequency-tripled Nd:YAG laser at 355 nm
- Fiducial Marks – minimal protrusion into the airflow (< 10 μm), generated at low laser power (40 mW, one pass)
- Microfence Elements – protrude into the airflow (50-150 μm), generated at high laser power and several passes

Microfence Template Generation

Heated Press

Controlled Thickness

Laser Ablation

Controlled Material Removal

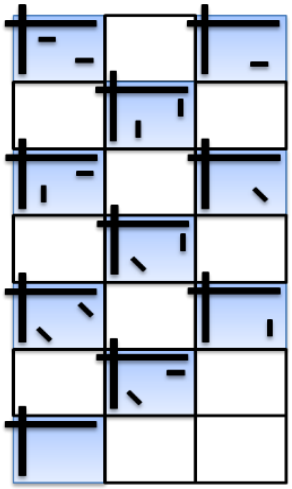

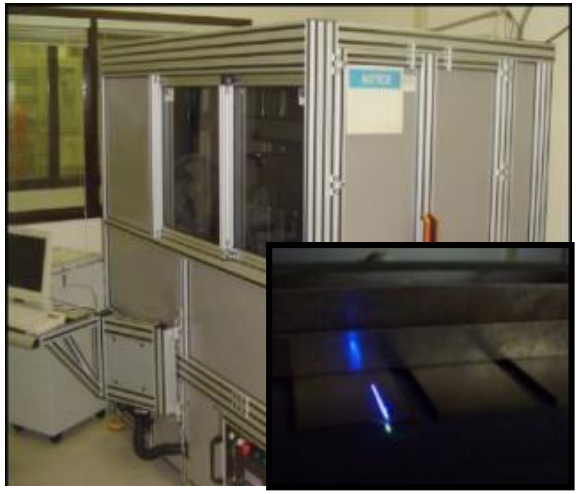

Sensor Generation-Soft Lithography

- Molded in a heated press under mild pressure and heating conditions (100 °F)
- Silicones (EcoFlex® series)

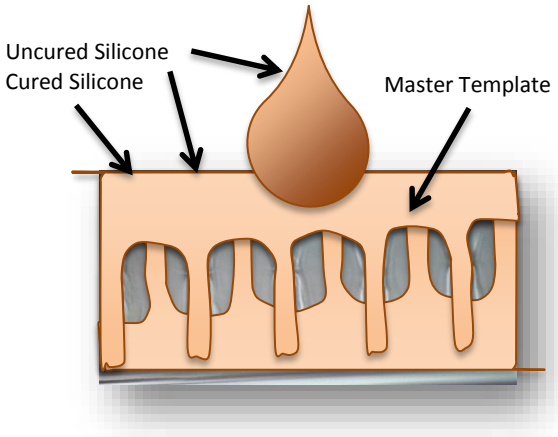

Silicone	Modulus, MPa	Tensile Strength, MPa
Sylgard 184[a]	1.84	7.07
Silastic T2[a]	1.50	5.52
EcoFlex 0050	0.08	2.14
EcoFlex 0030	0.07	1.38
EcoFlex 0010	0.06	0.83

Silicone Structures

- 400 mW, 8 Passes
- 600 mW, 4 Passes

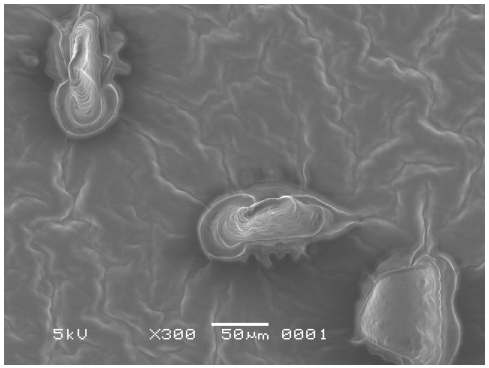

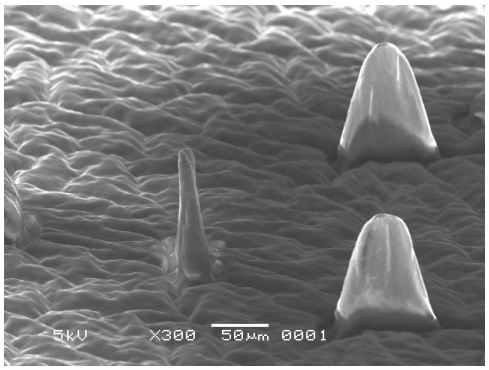

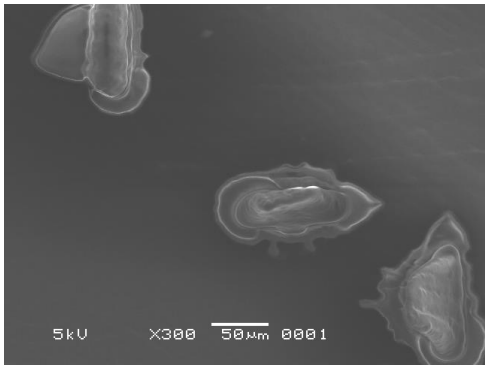

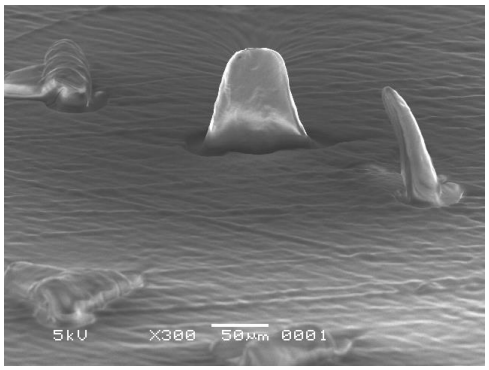

Balance between sensitivity and stability:

- Tall, narrow features generated from low modulus materials
- Features that maintain shape and orientation under static conditions

Silicone Structures

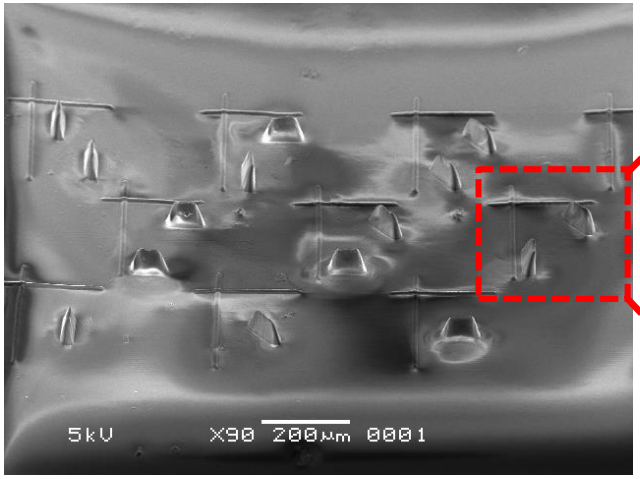

Wide view of multiple dies

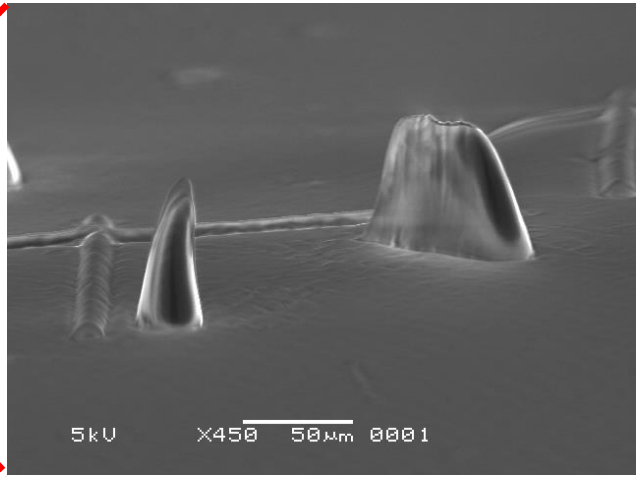

Higher magnification of a single die

Fluorescent Labeling

- Deposit rhodamine B on template
- Remove excess using a squeegee
- Cast silicone

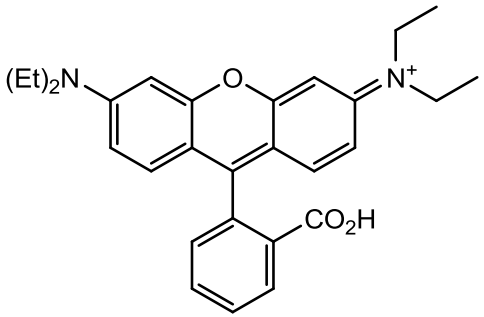

Rhodamine B

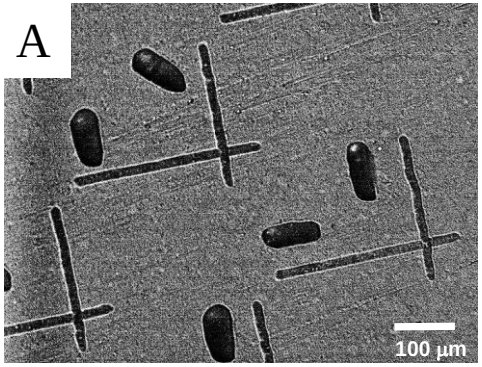

White light image

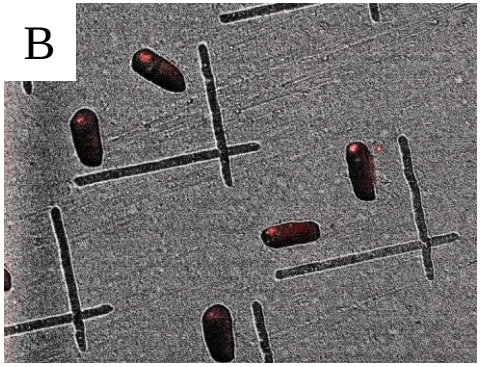

Composite image

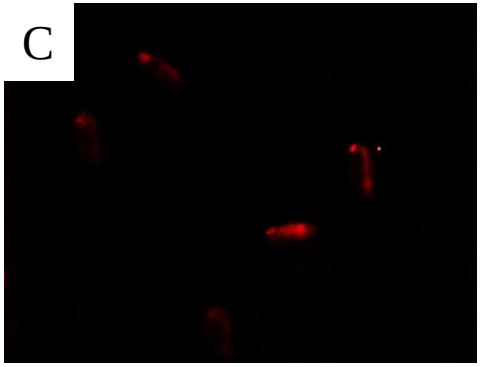

UV light image

Sensor Prototype

- Optical microscope hardware provides lighting and resolution to detect deflection of sensing element

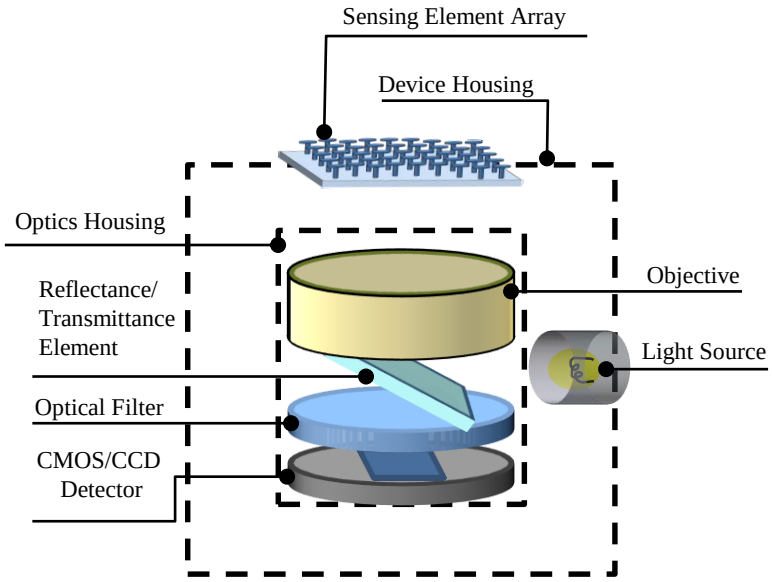

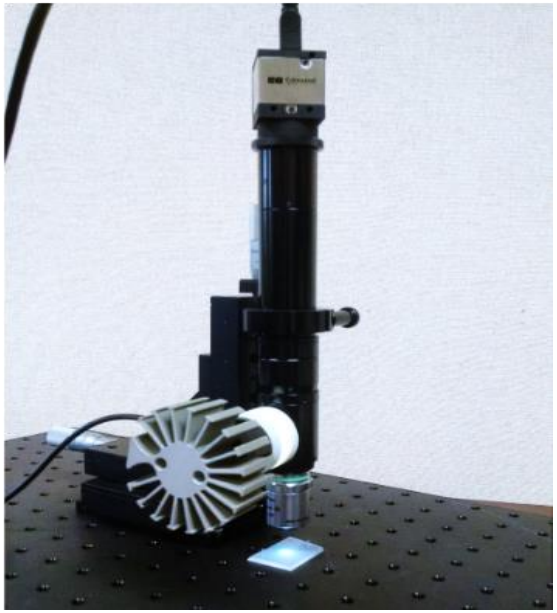

Note: Instrument is inverted here

Laboratory Bench Testing

- Compressed gas jet
- Deflection visible to the eye
- Video of the experiment allows measurement (yellow arrows)

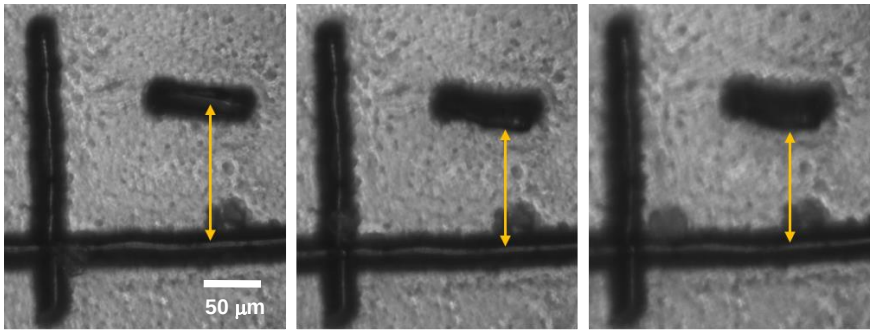

Moderate Jet: Decrease of about 14%
Full jet: Decrease of about 19%

Microfence Deflection

Free-jet tests (outside wind tunnel)

- The following video (with enhanced contrast) shows the visible deflection in the presence of a free-jet stream of compressed gas:

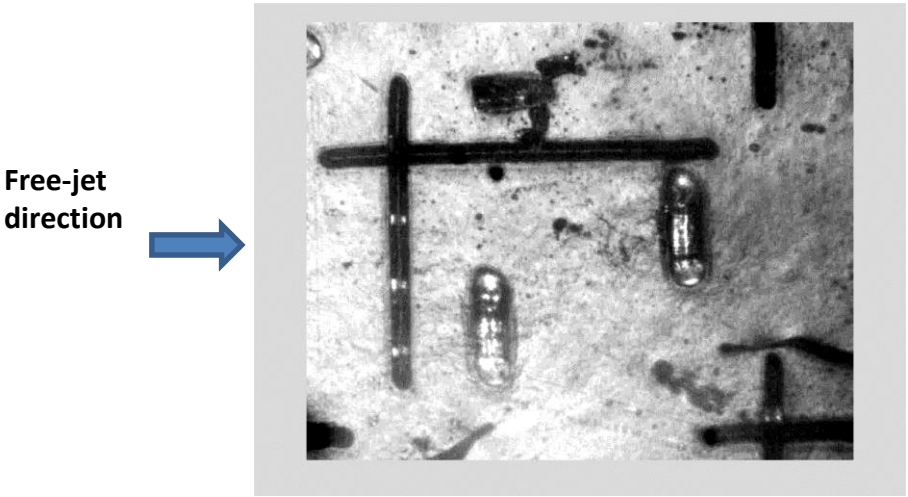

Digital image correlation is employed to get an estimate of the deflection in pixels

Digital Image Correlation (DIC)

- Employ correlation to measure shifts in datasets (images)
- Compare intensity between corresponding blocks or subsets of pixels
- Extract a displacement mapping function to track the deflection of the microfence tip

Free-jet direction

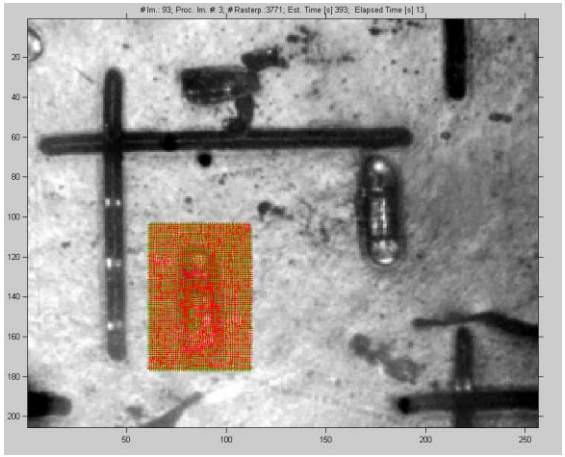

The pixels tracked for digital image correlation

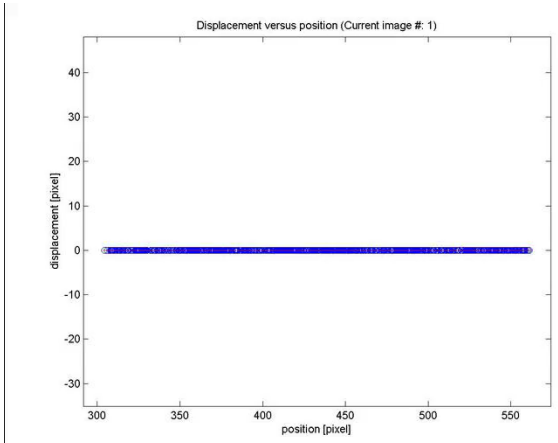

The video shows the displacement (pixels) of the bulk of the tracked points

Wind Tunnel Testing

Initial tests with first generation model at NCSU low speed wind tunnel

- Objective:
  - Debug sensor installation and vibration problems
  - Refine sensor characteristics (sensor height, flexibility, aspect ratios, etc.)
  - Conduct a qualitative assessment of microfence deflection in the wind tunnel
- First generation model:
  - Designed with a flat plate having a hemispherical leading edge
  - Sensors were installed on a quartz disk (≈3.2 cm diameter)
  - Microscope housed in a support structure and blocked from direct interaction with the airflow

Shear Stress-Velocity Relationship

Turbulent flow solutions

- The velocity range used here in m/sec corresponds to a range of 30 – 90 ft/sec in the NCSU wind tunnel.
- These plots are for the current fixed position of the sensor (9 inches or 0.2286 m).

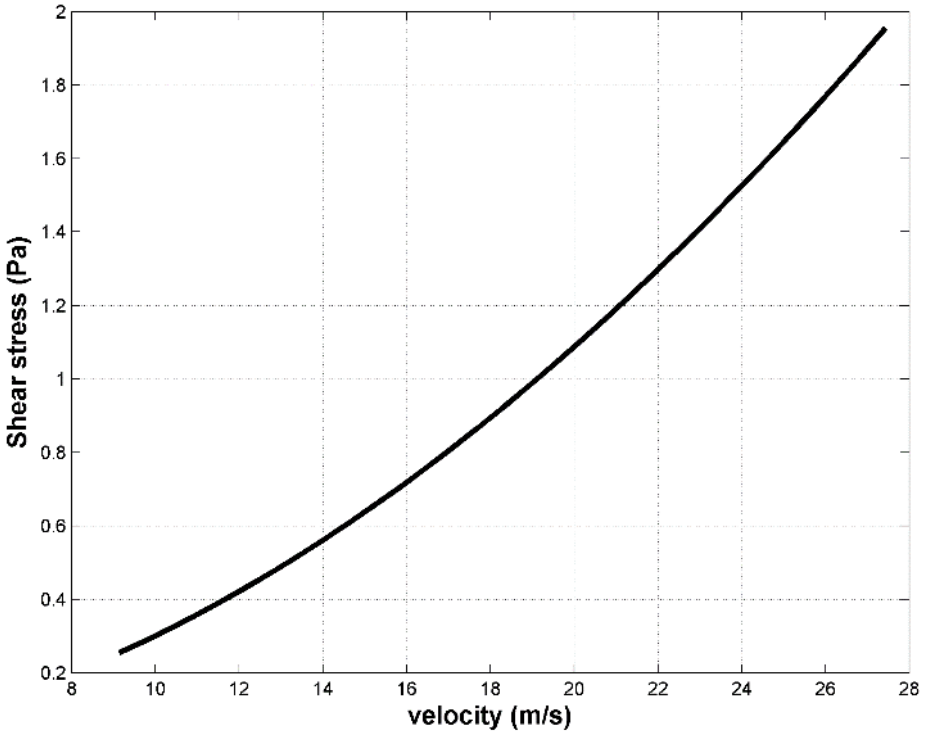

"Schlichting, H. (1979) *Boundary-Layer Theory* McGraw Hill, New York, U.S.A.".

Viscous Sublayer Layer Thickness

Turbulent flow solutions

- The velocity range used here in m/sec corresponds to a range of 30 – 90 ft/sec in the NCSU wind tunnel.
- These plots are for the current fixed position of the sensor (9 inches or 0.2286 m).

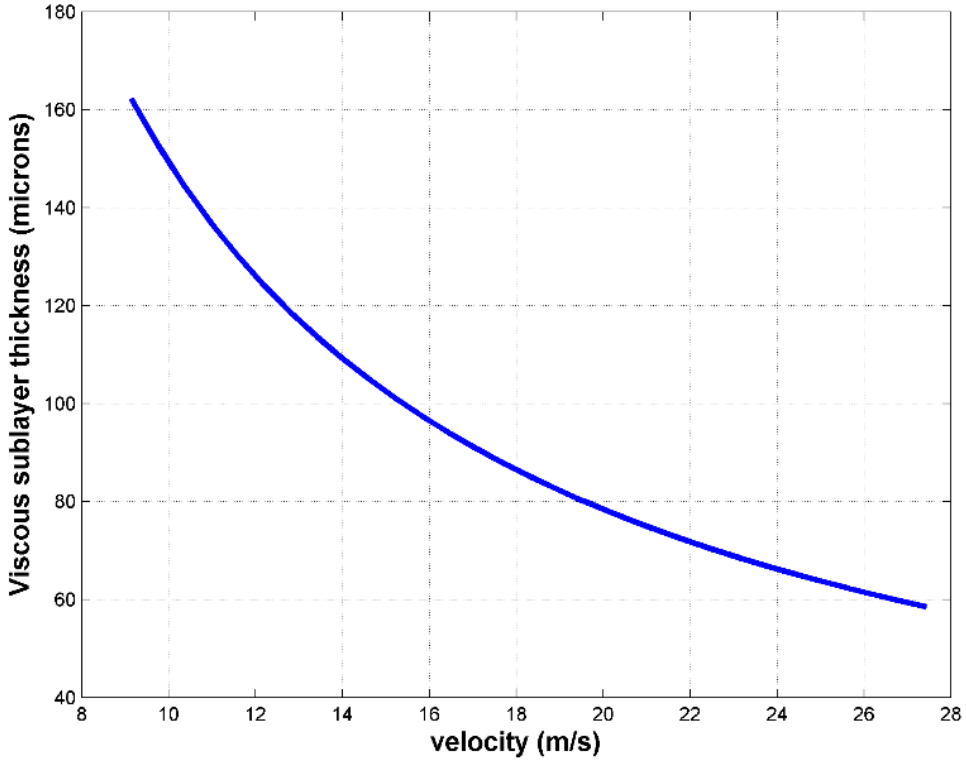

"Schlichting, H. (1979) *Boundary-Layer Theory* McGraw Hill, New York, U.S.A.".

Boundary Layer Thickness

Turbulent flow solutions

- The velocity range used here in m/sec corresponds to a range of 30 – 90 ft/sec in the NCSU wind tunnel.
- These plots are for the current fixed position of the sensor (9 inches or 0.2286 m).

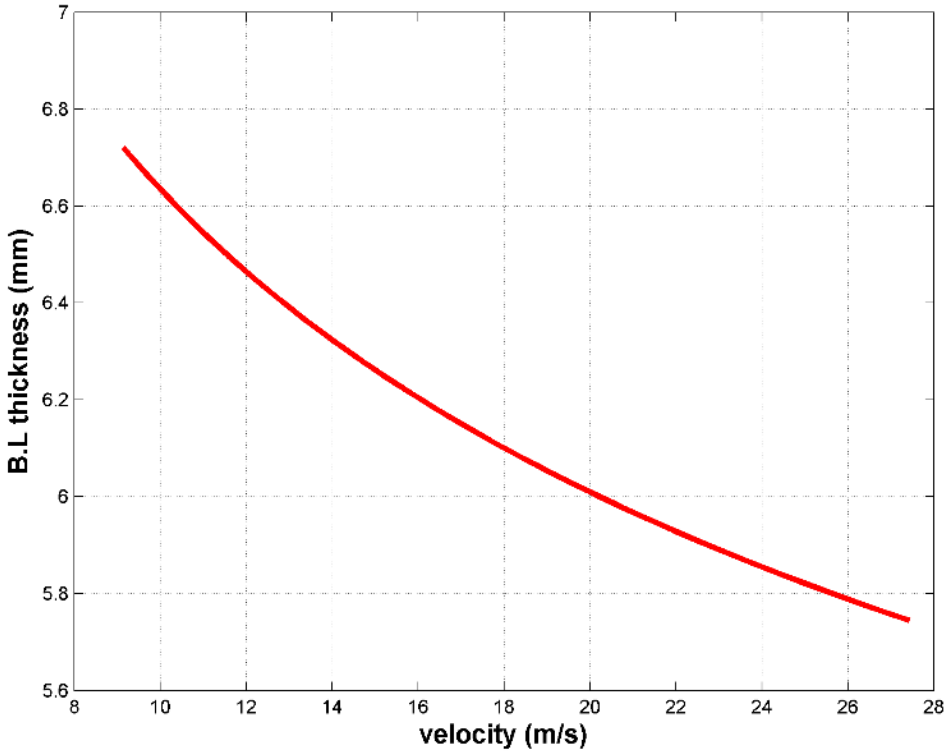

"Schlichting, H. (1979) *Boundary-Layer Theory* McGraw Hill, New York, U.S.A.".

Boundary Layer Thickness

Turbulent flow solutions

- The velocity range used here in m/sec corresponds to a range of 30, 50, 70 and 90 ft/sec in the NCSU wind tunnel.
- X-axis is the distance from the leading edge (L.E.)

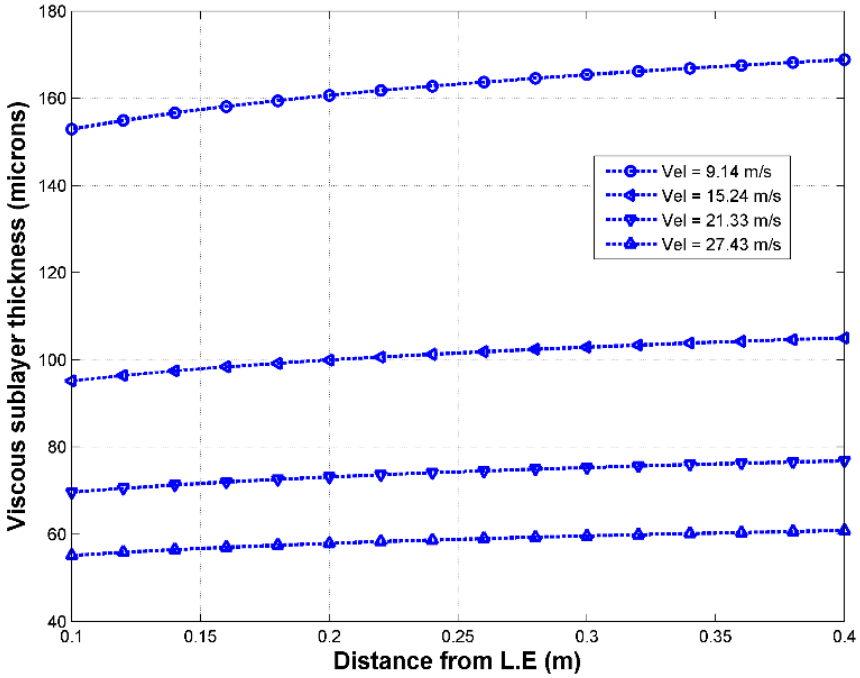

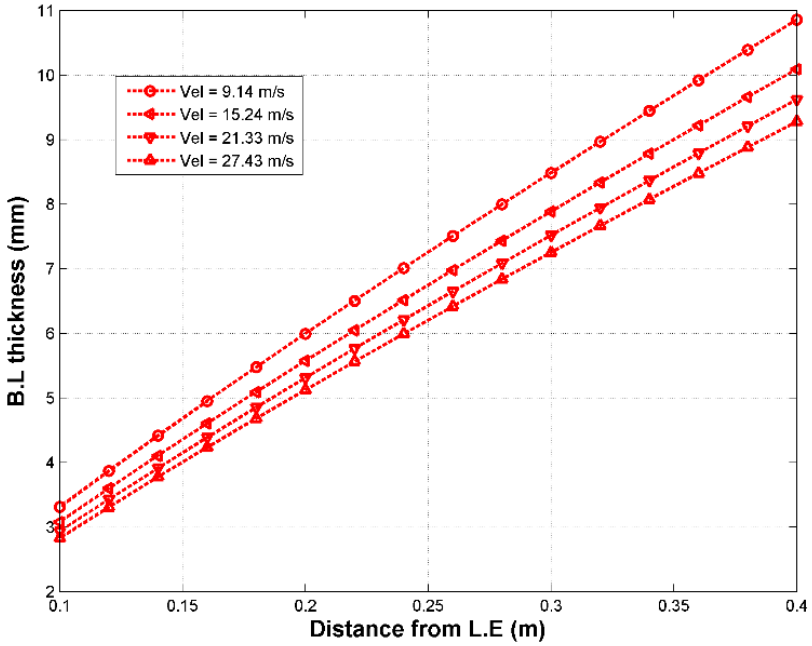

"Schlichting, H. (1979) *Boundary-Layer Theory* McGraw Hill, New York, U.S.A.".

First Generation Model

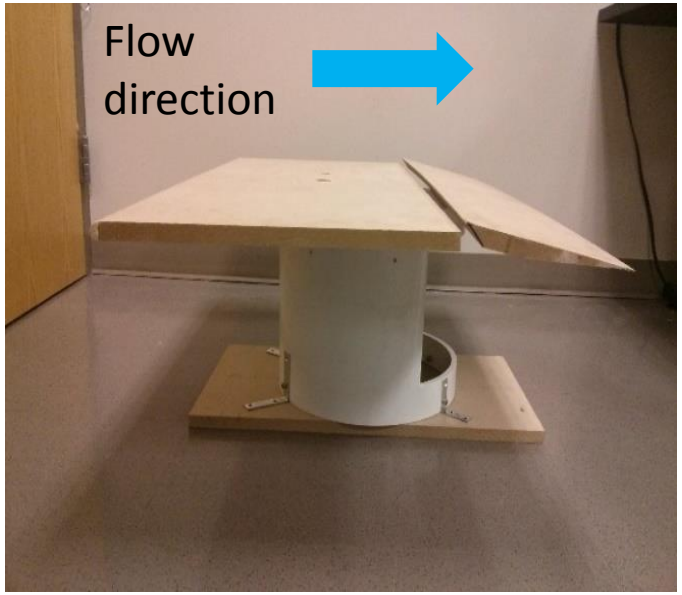

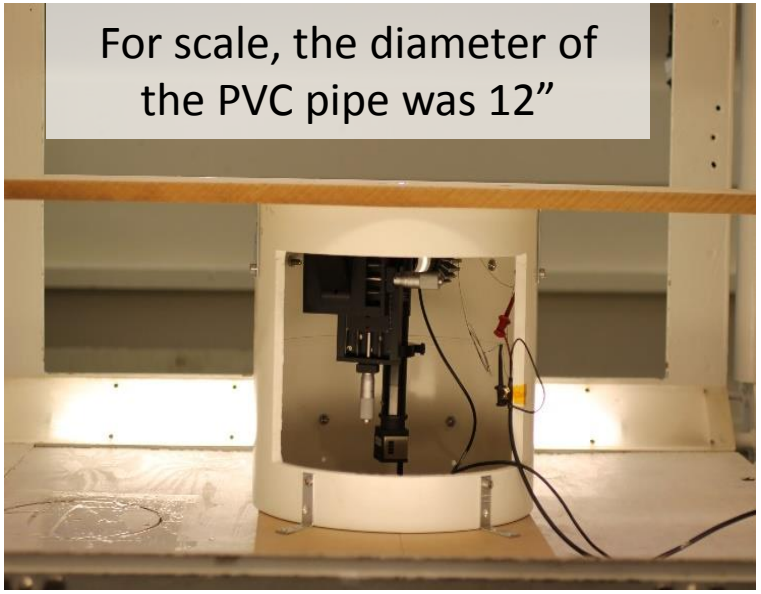

Flow
direction

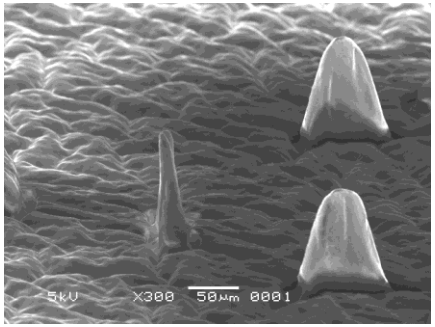

Wind Tunnel Testing

- Image Enhancement

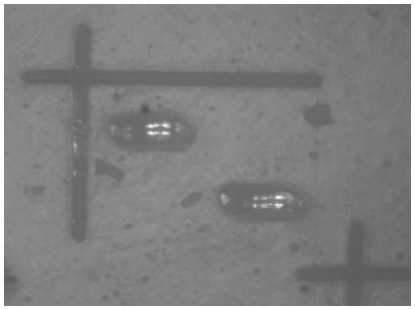

A raw image captured by the camera

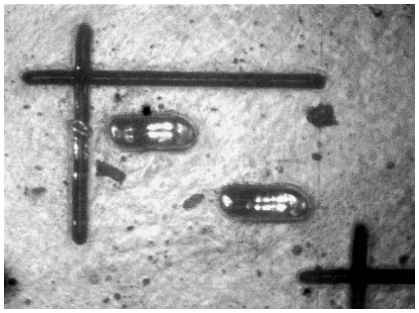

An enhanced image with greater contrast

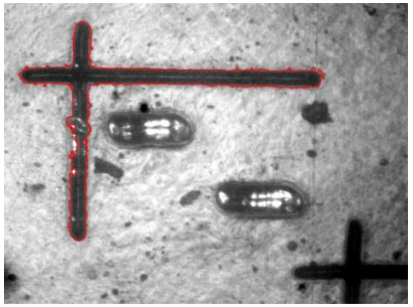

Reference features, in red, were tracked by the algorithm

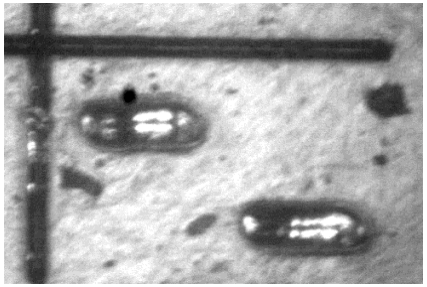

The final re-sized and re-aligned image based on the tracked reference

Wind Tunnel Testing

- Digital Vibrational Stabilization

Freestream velocity = 29 m/sec

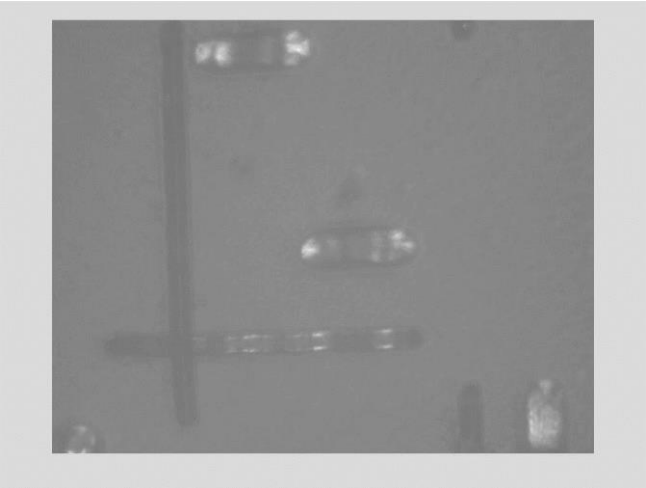

Raw video captured from the wind tunnel

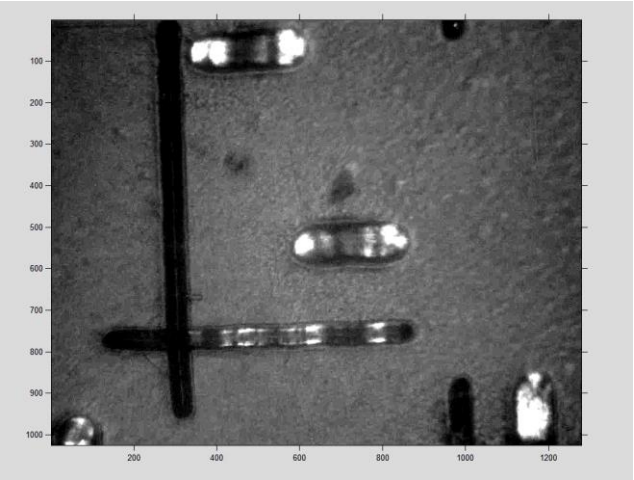

Stabilized video with contrast enhancement

Wind Tunnel Testing

- Test conditions:
  - EcoFlex 0010 pillars
  - v=31.83 m/sec

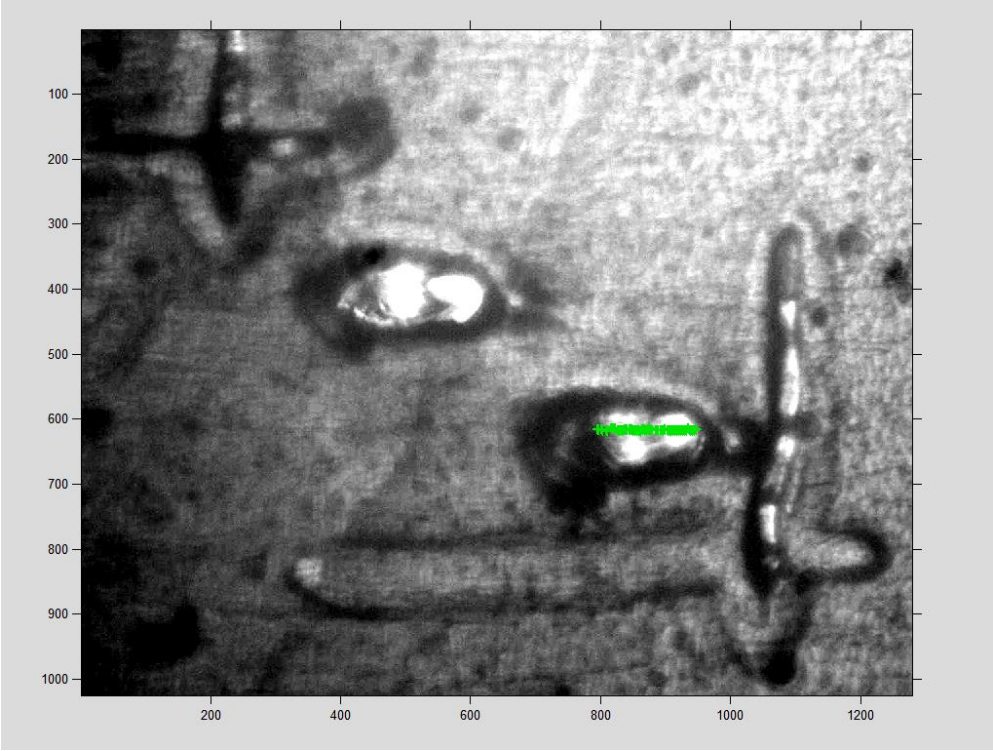

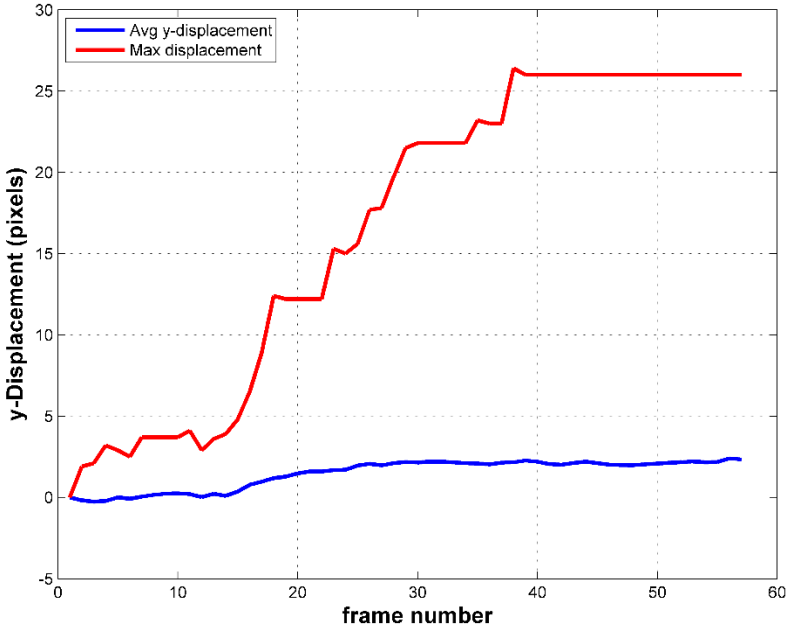

Data collected on 10/17/2015!!!

Wind Tunnel Testing

- Time-resolved Deflection of EcoFlex 0010 pillars ~100 μm tall

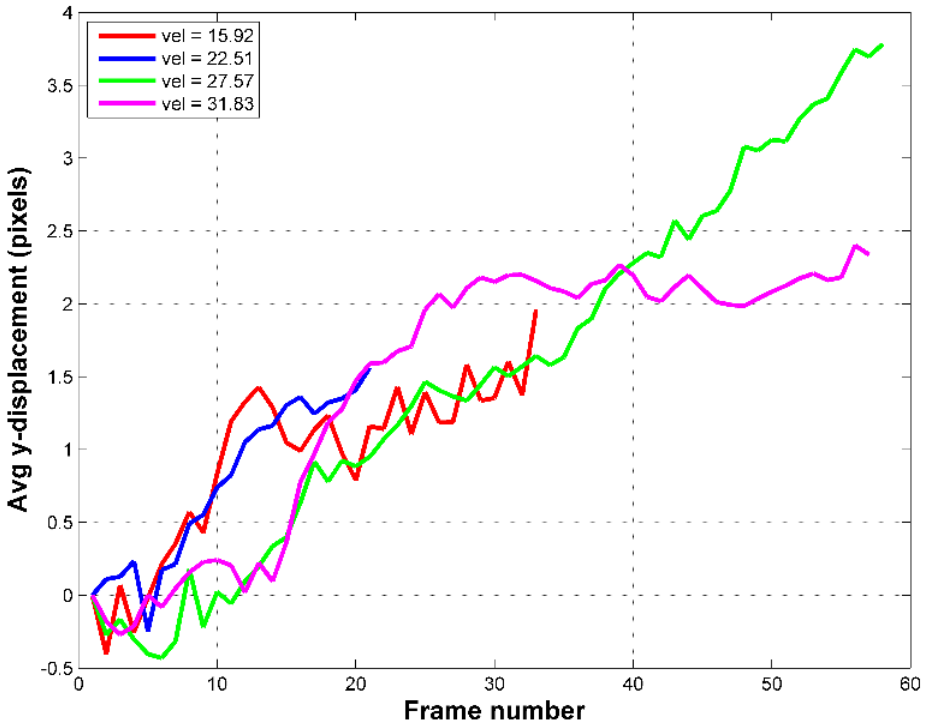

Data collected on 10/17/2015!!!

Wind Tunnel Testing

- Maximum Deflection of EcoFlex 0010 pillars ~100 μm tall

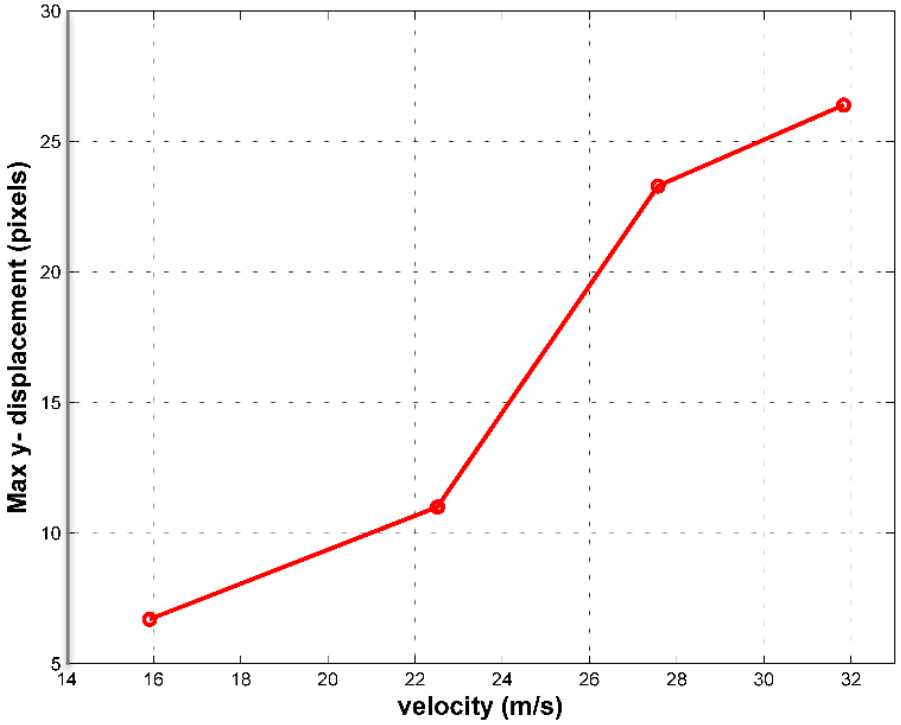

Data collected on 10/17/2015!!!

2nd Generation Model

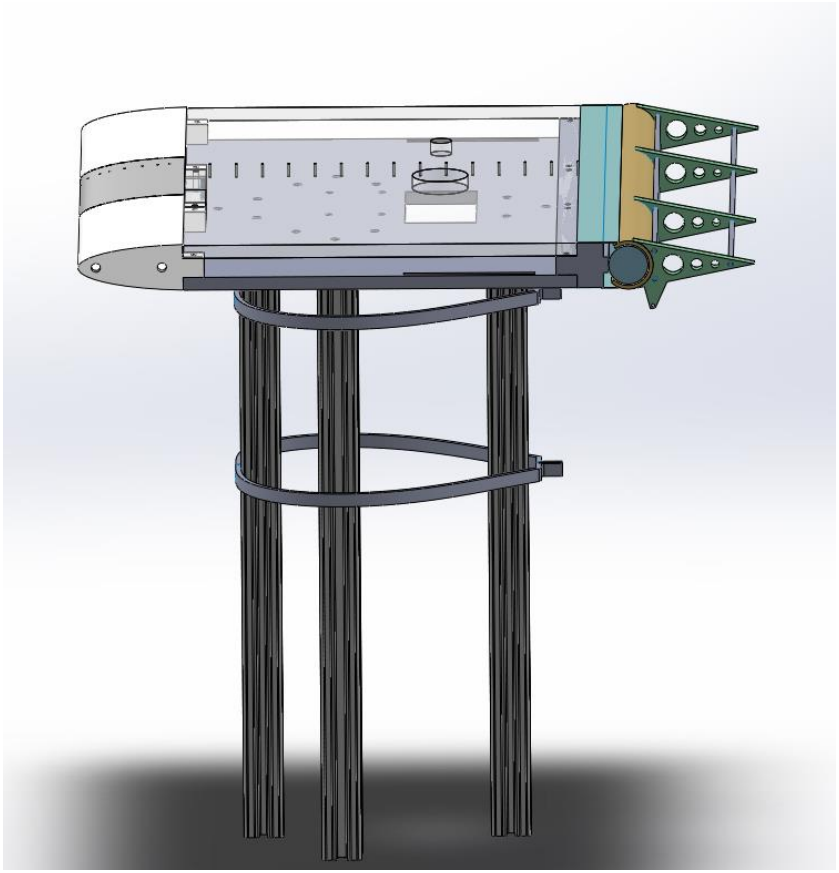

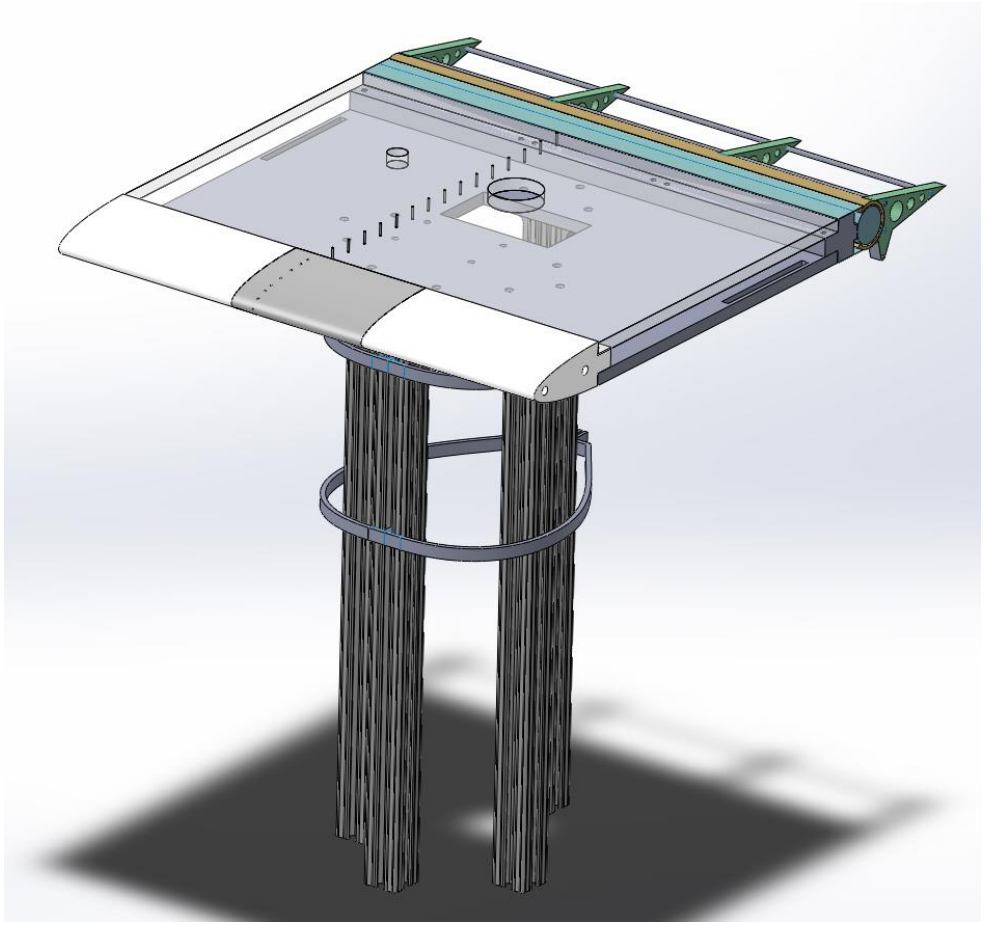

2nd Generation Model-Design

Fabrication Update 10/28/20015

1. Elliptical leading edge –
   - 3D printed

Status : Printed and shipped (Not received yet)

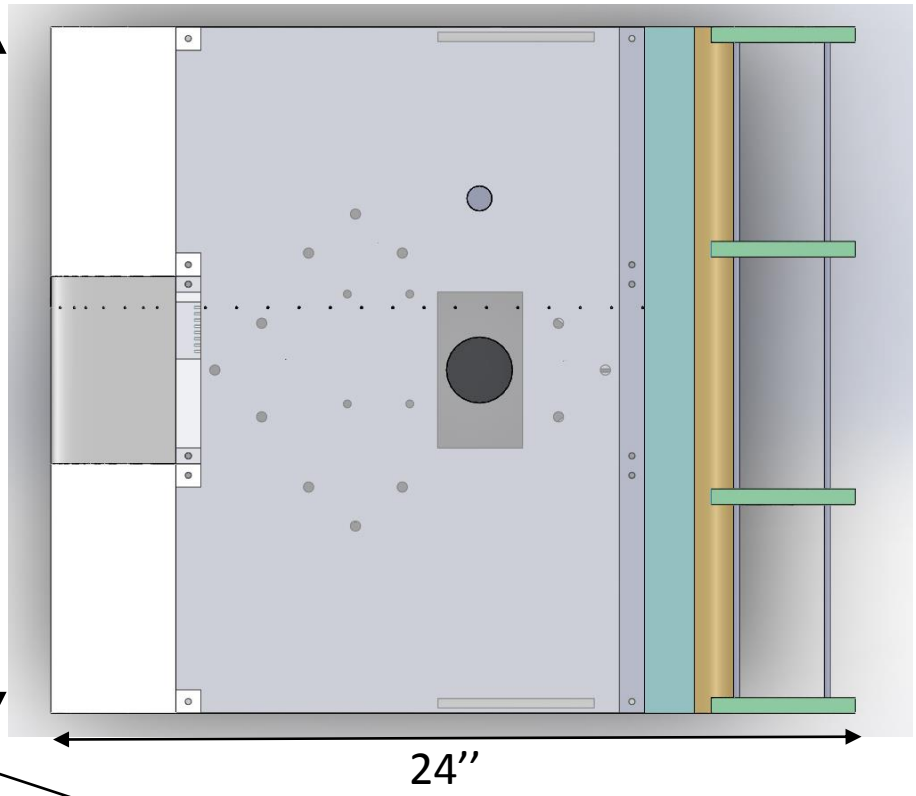

2. Upper surface Acrylic sheet (0.5'' thickness)

Status : Designed, not yet ordered

3. Lower surface Aluminium plate (0.5'' thickness)

Status : Being machined

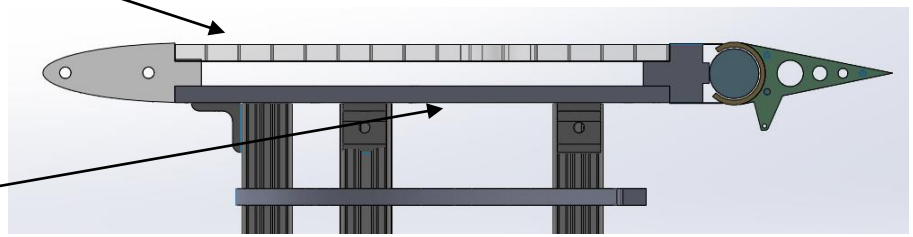

2nd Generation Model

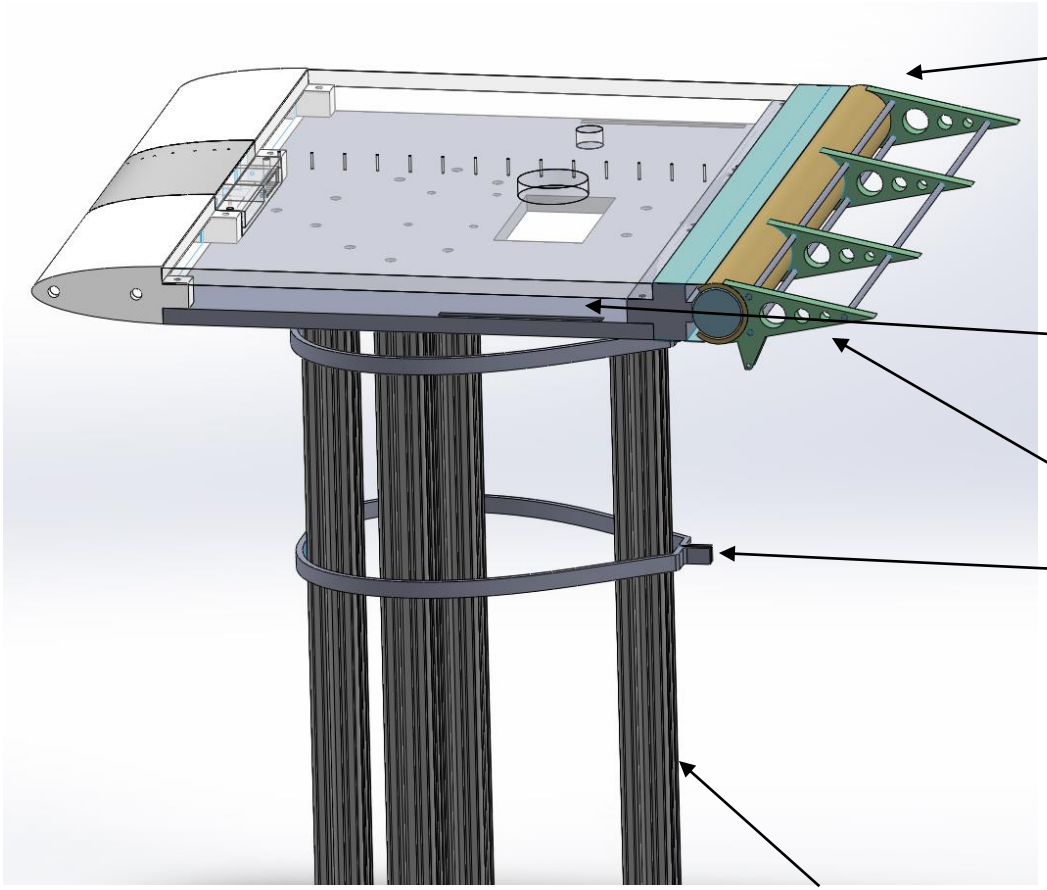

4. Flap mechanism

Status : Designed and being constructed

- The lower surface plate with holes for mounting brackets and camera
- Ribs for the flap
- Ribs for support fairing

Status : Designed and being cut by waterjet

5. Aluminum Extrusions for support and base structure

Status : Ready

2nd Generation Model-Components

3D printed Leading Edge

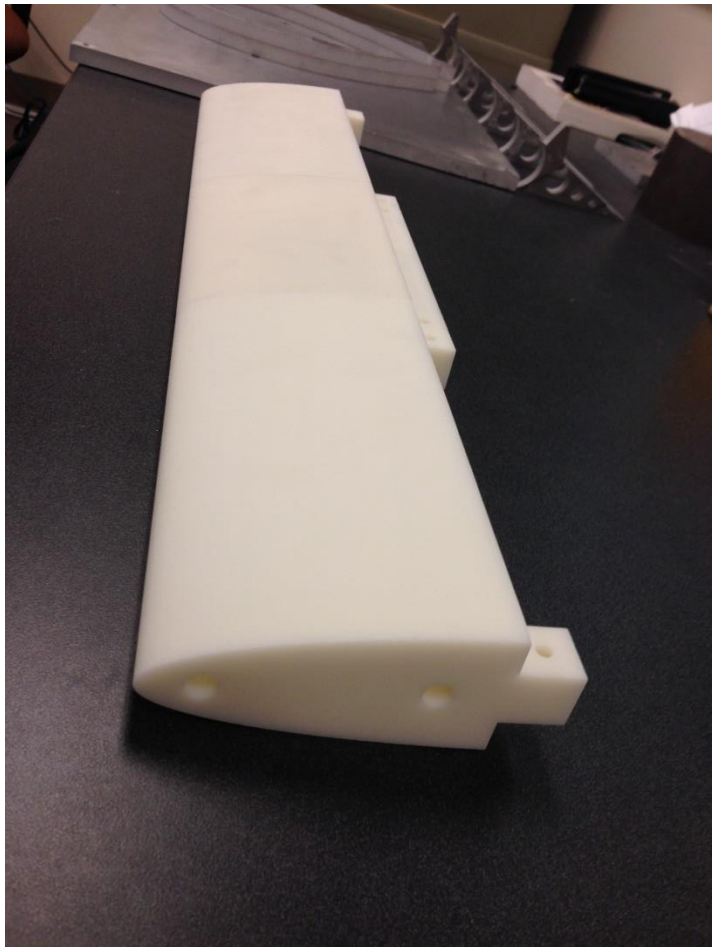

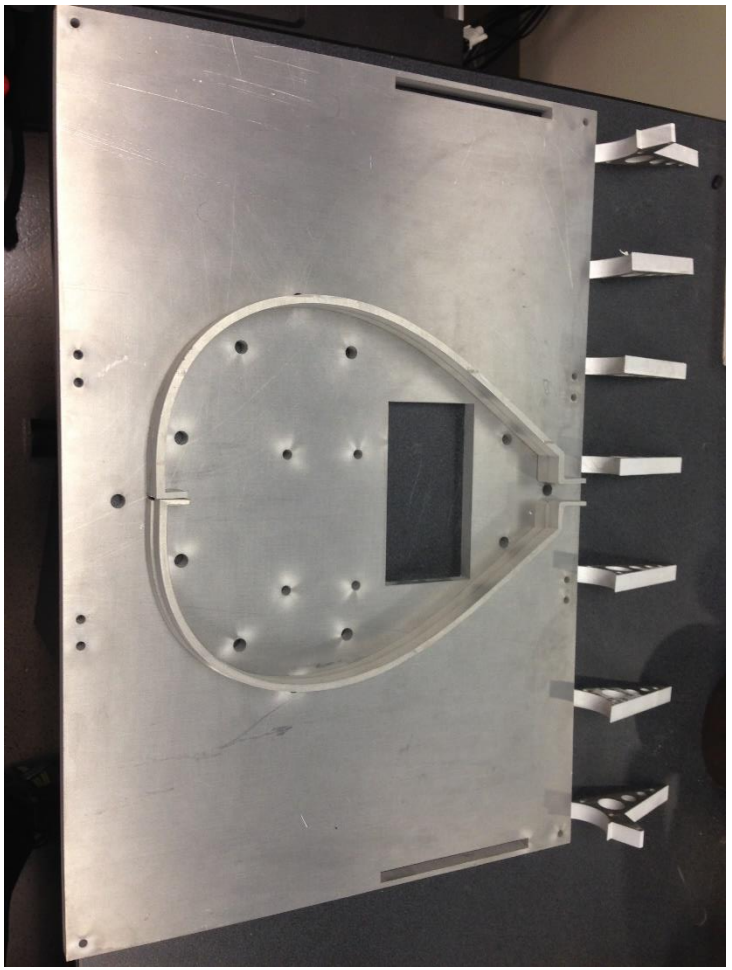

2nd Generation Model-Components

Ribs for support fairing

Ribs for the flap

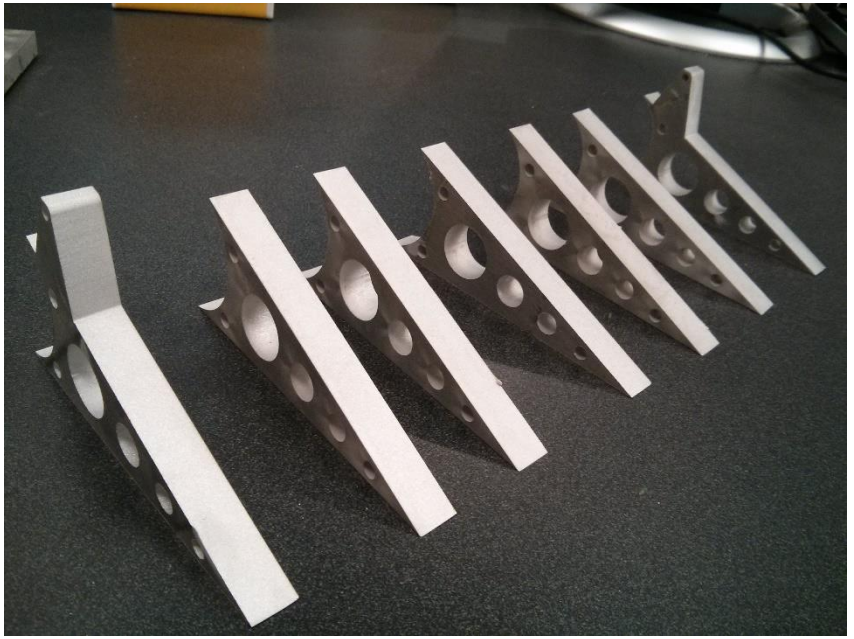

2nd Generation Model-Sample Elevator

- Sensor disk must be aligned with top surface of the flat plate to prevent flow disturbance or protrusion above the viscous sublayer
- Elevator mechanism allows adjustments without removing flat plate
- The tolerances of this design were considered for compatibility with 3D printing technology

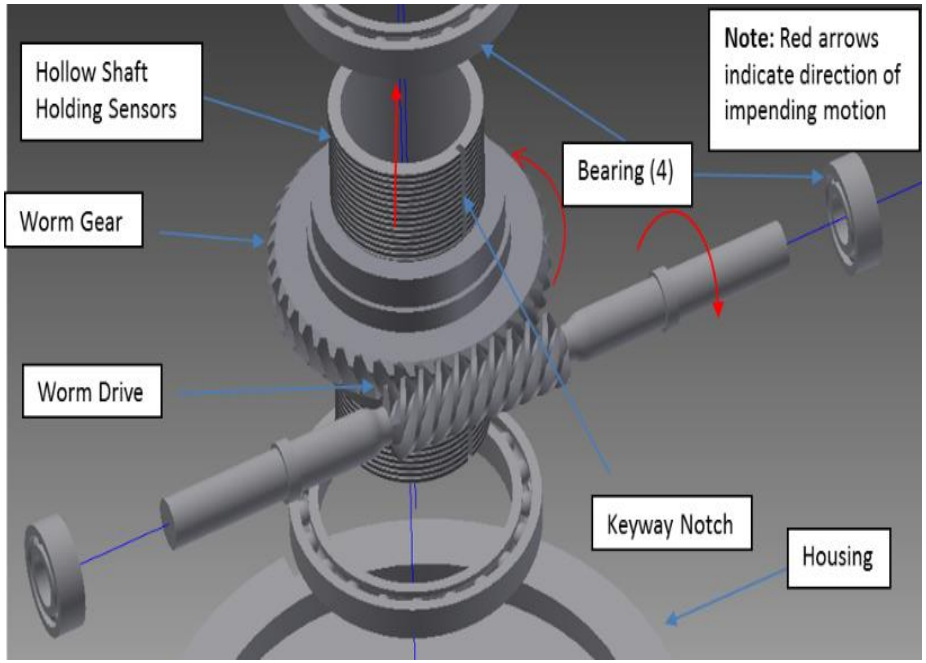

Exploded view

For scale, the hollow shaft has an inner diameter of 1.325”

2nd Generation Model

- Boundary Layer Rake

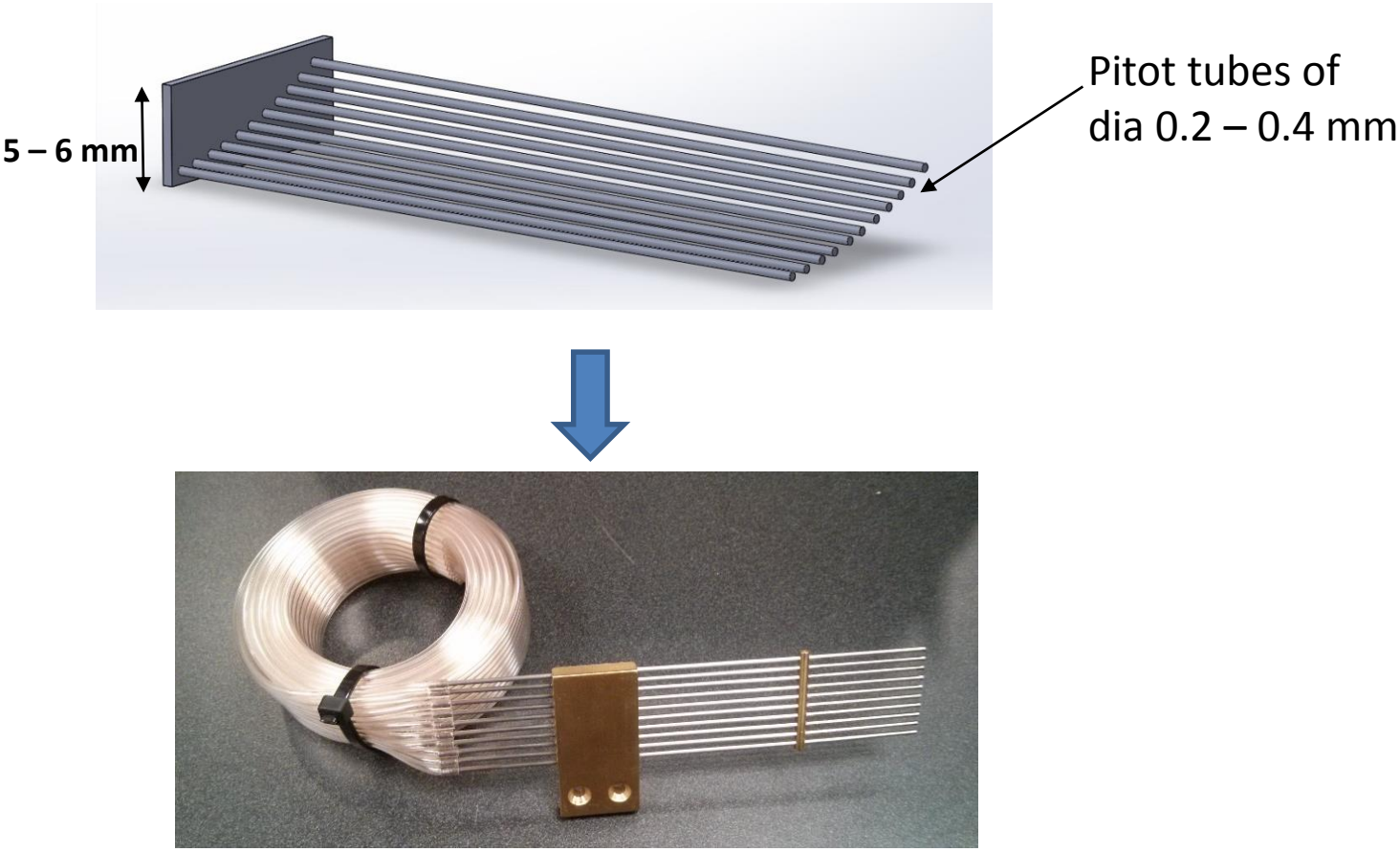

Other Sensor Designs- Capacitance Change

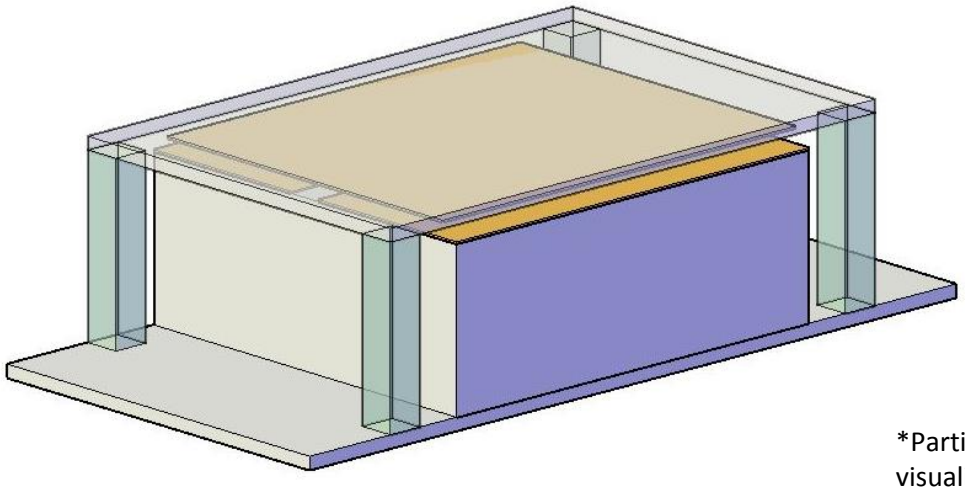

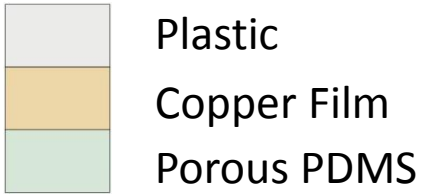

*Partial transparency to aid in concept visualization

Principles:

- Under airflow, the top pillar-supported plates will shift, causing a difference in the overlapped area between the top and bottom two copper plates
- A capacitance difference between the bottom two plates will be indicative of the degree of displacement

Capacitance Change Sensor

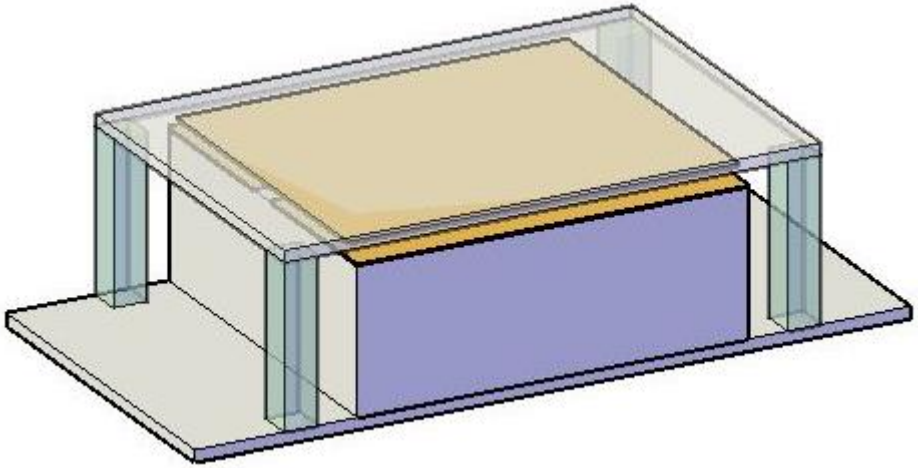

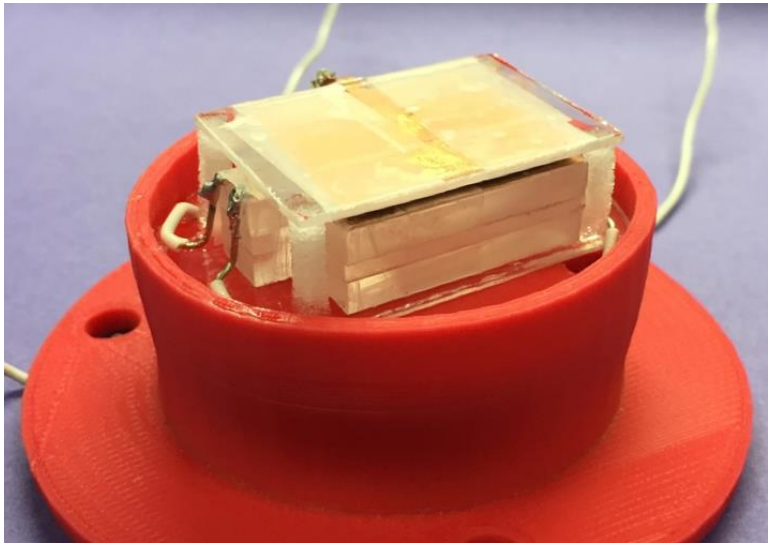

Holder for placing the sensor in the flat plate for wind tunnel testing.

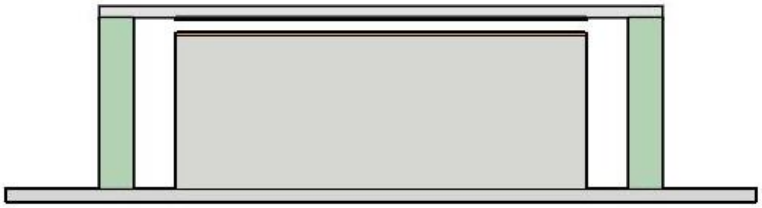

Side View

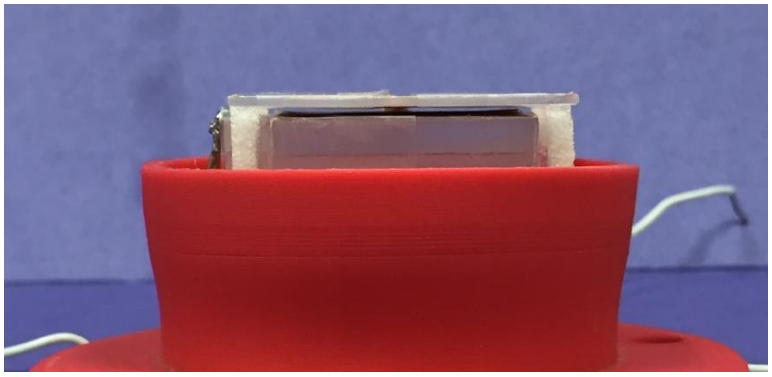

Capacitance Change Sensor

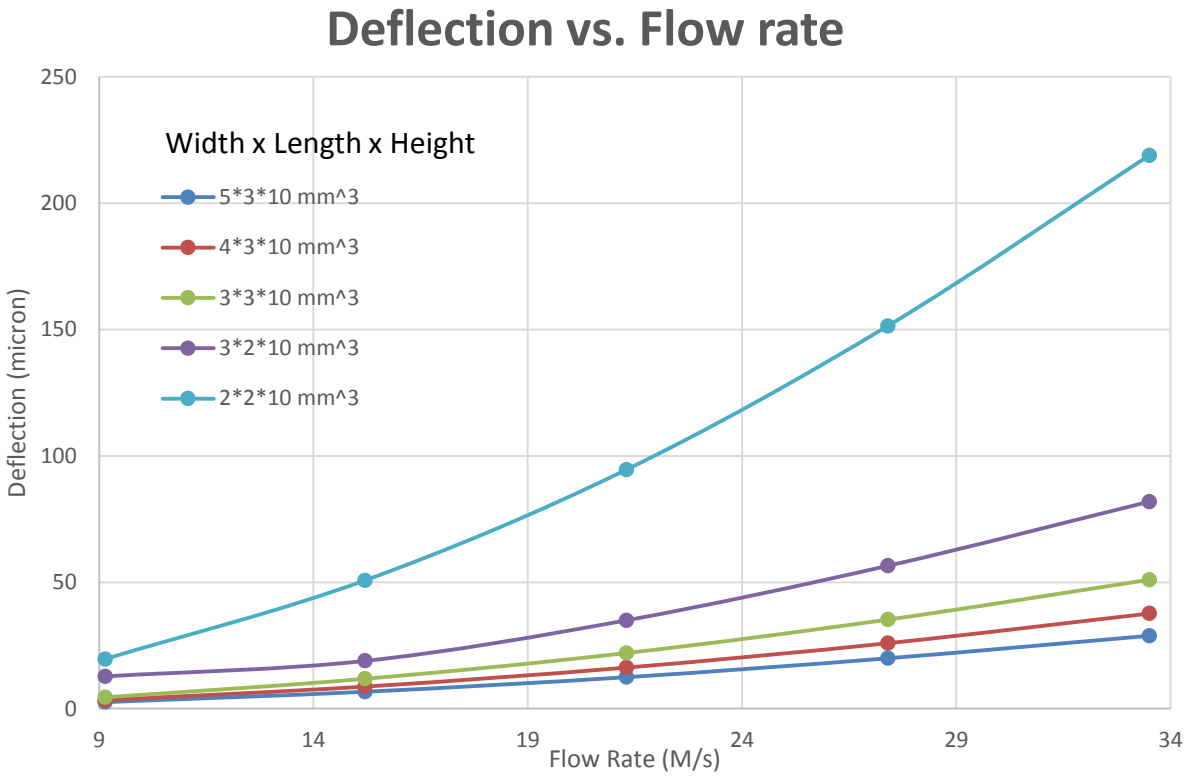

Flow Rate (m/s)	Shear Stress (Pa)
9	2.70E-01
14	5.97E-01
19	1.03E+00
24	1.58E+00
29	2.22E+00
34	2.95E+00

Simulation was conducted to determine how much the pillar supports (with different dimensions) deflect under turbulent air flow

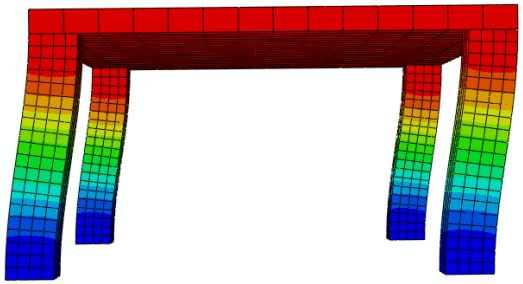

Capacitance Change Sensor

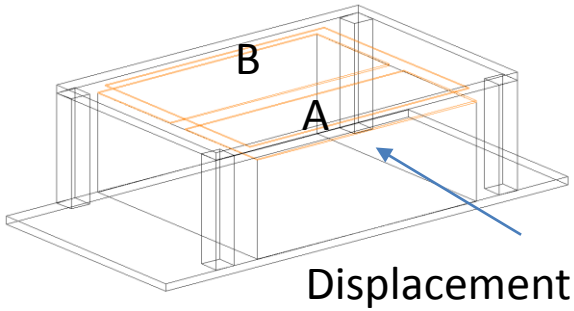

Displacement Direction

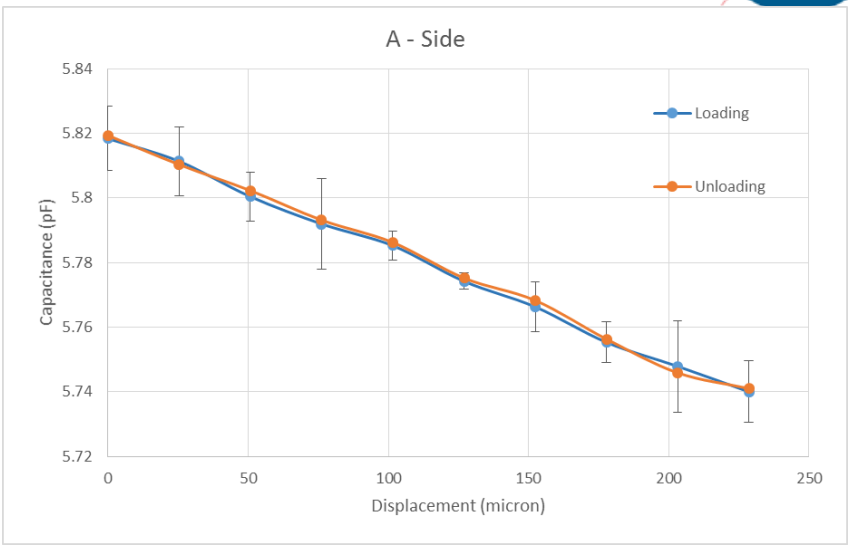

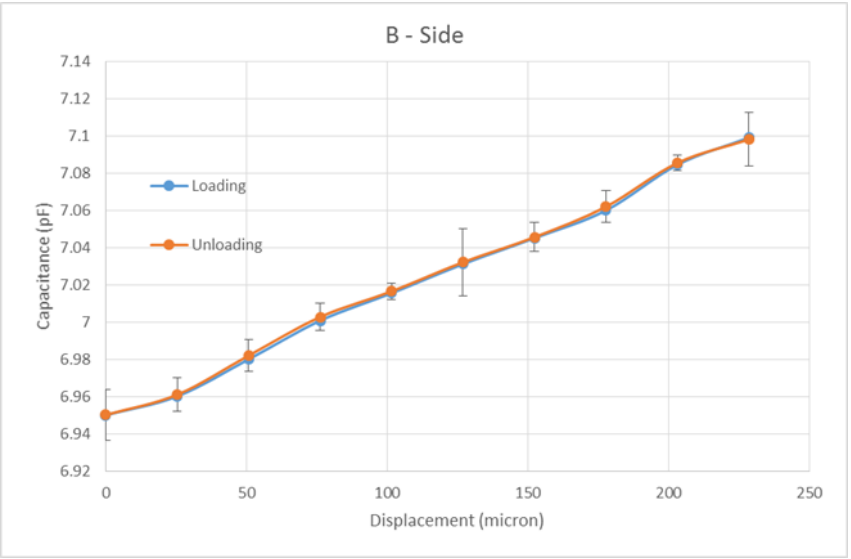

Other Sensor Designs- Piezoelectric

- Direct piezoelectric effect
  - Mechanical -> Electrical

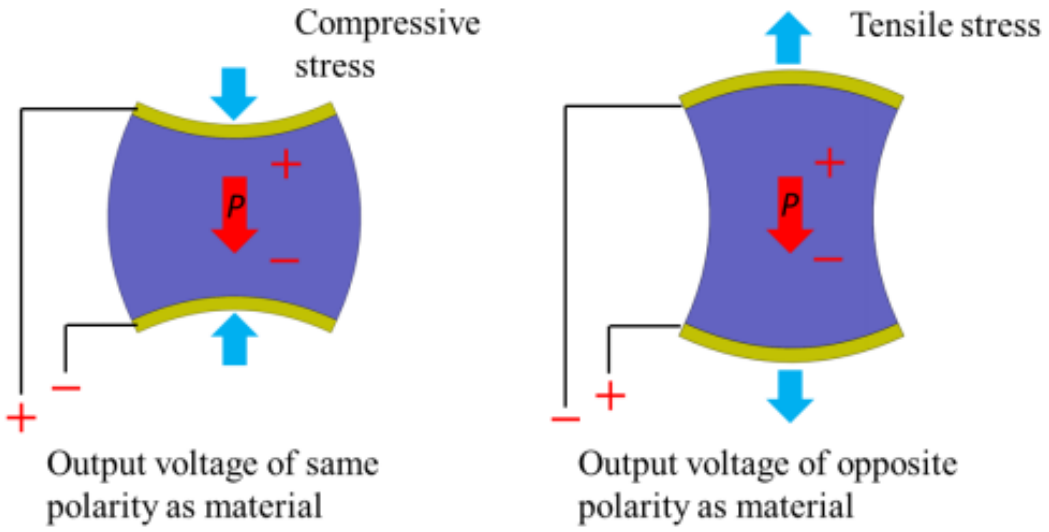

Other Sensor Designs- Piezoelectric

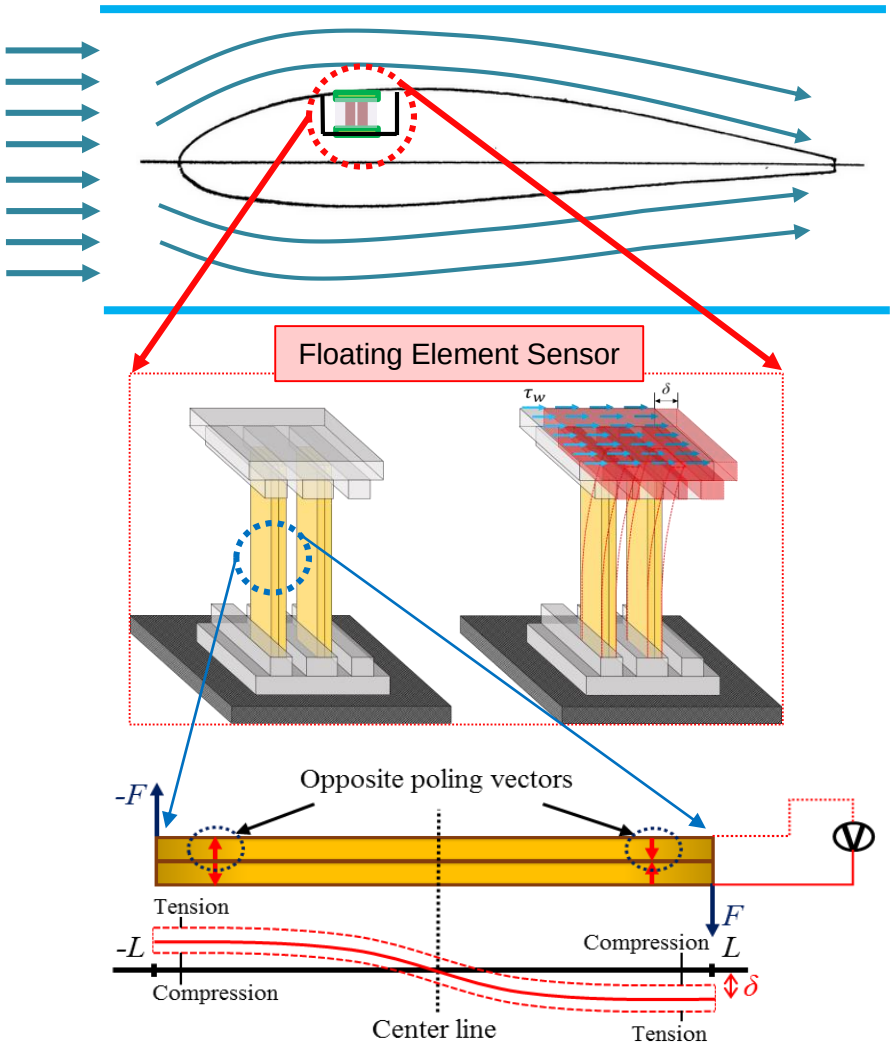

Piezoelectric Sensor

- Process of fabrication

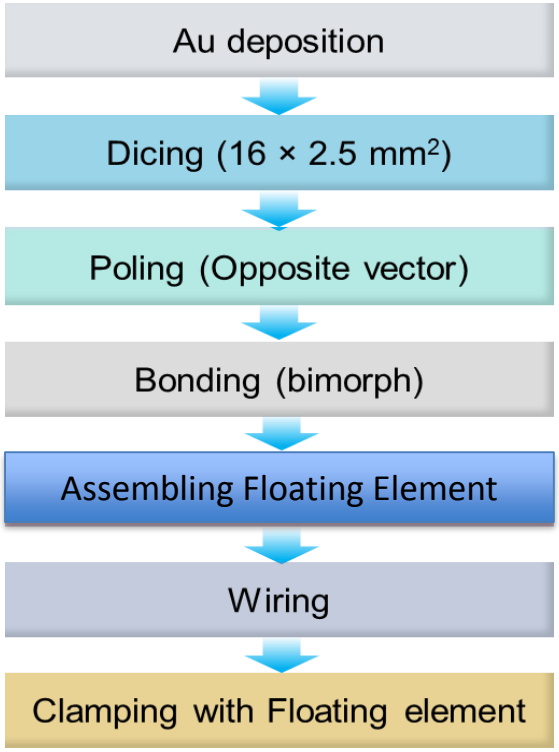

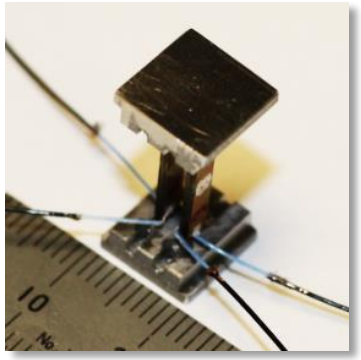

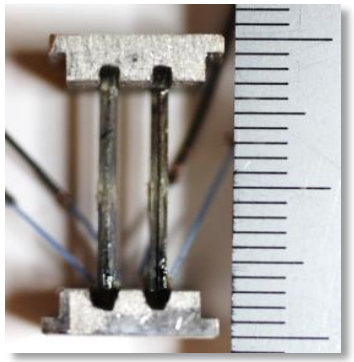

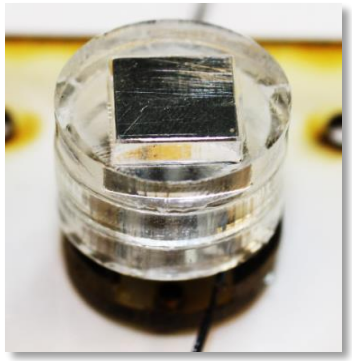

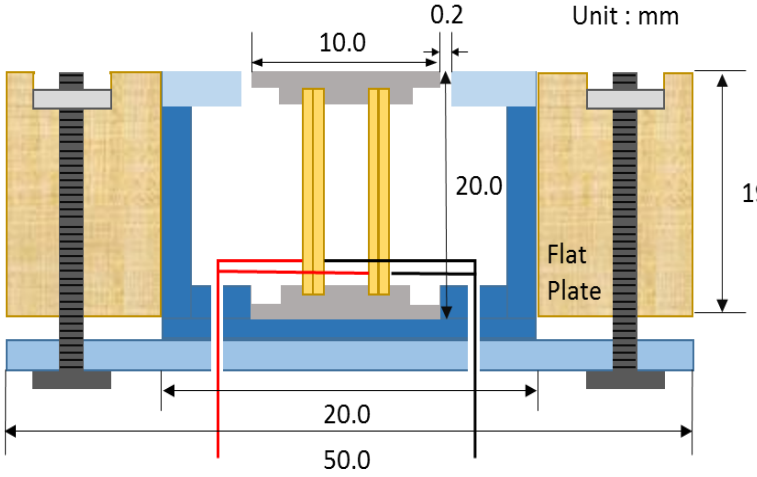

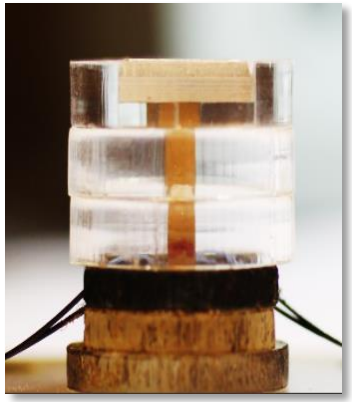

Piezoelectric Sensor

- Sensor Calibration

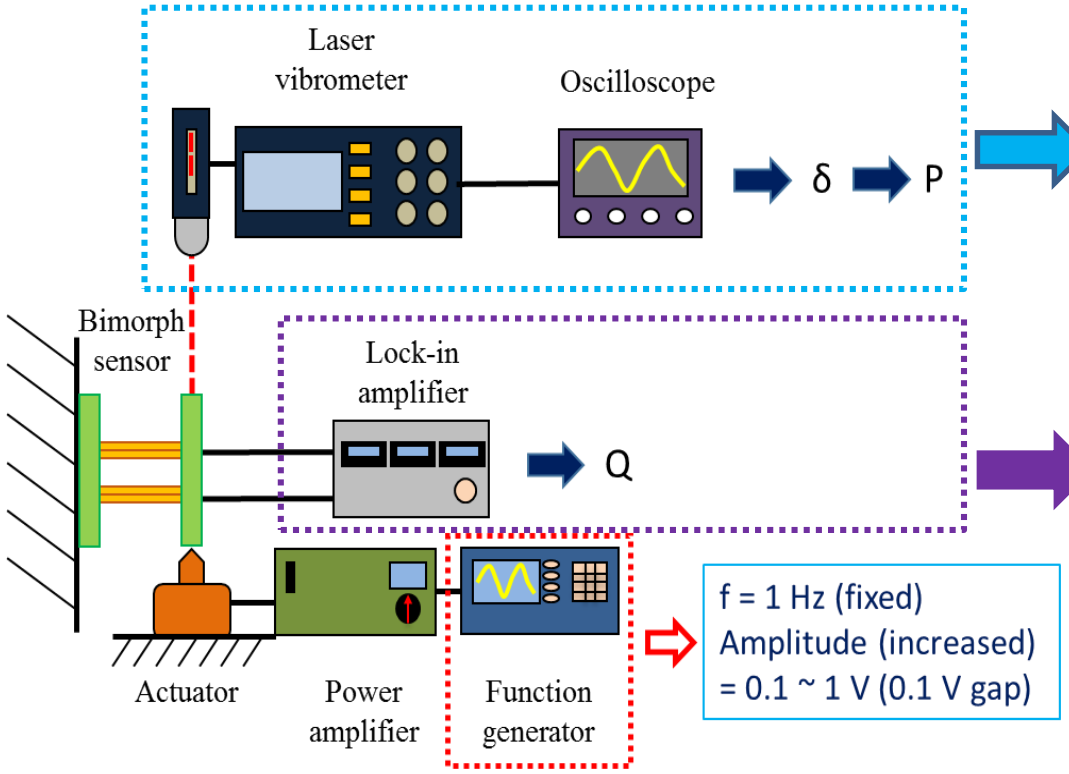

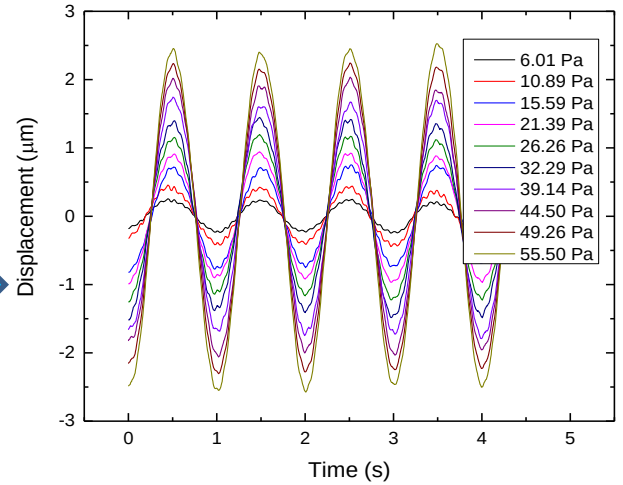

Peak to peak displacement from laser vibrometer

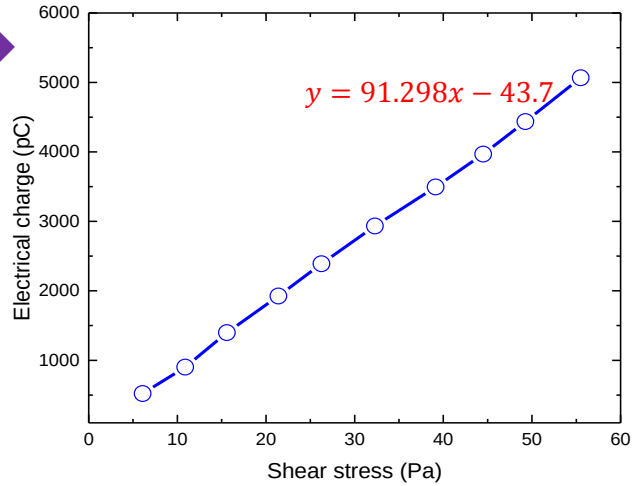

Electrical charges as function of shear pressures

Other Sensor Designs- Macropillar

- Assisted Mehti Koklu in Flow Physics and Control Branch (LaRC) in fabrication of macro-scaled pillars for flow detection

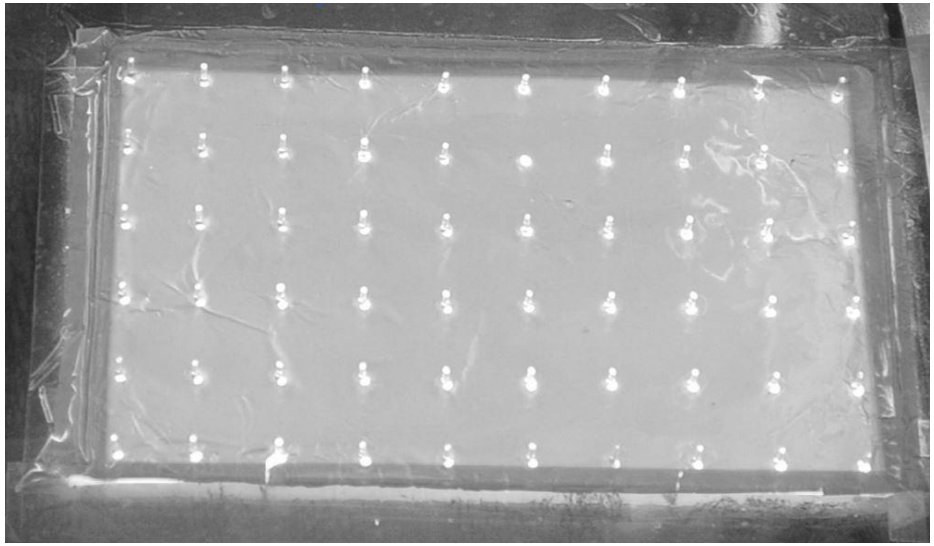

Approximately 6” × 3”

Other Sensor Designs- Macropillar

- Assisted Mehti Koklu in Flow Physics and Control Branch (LaRC) in fabrication of macro-scaled pillars for flow deflection detection

- Sensor array fabricated using vacuum bag technology from a much softer silicone
- Tip contrast enhanced by infusion of fluorescent dye

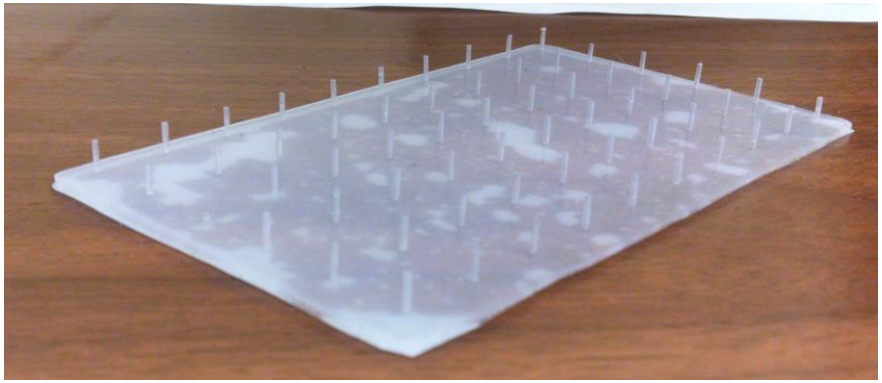

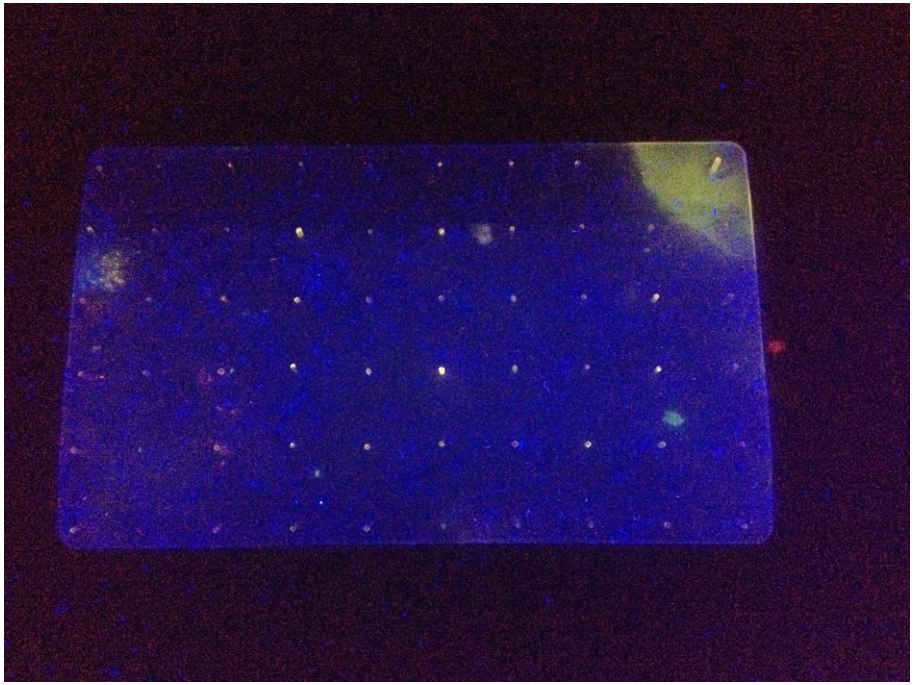

Next Steps

- Period of Performance (POP) for NCSU extended to 06/2016
- Spring NIFS intern, funded using branch resources, will continue supporting this work
- Extensive wind tunnel testing of 3 sensors (microfence, capacitance, and piezoelectric) at NCSU
- Finalize fabrication and experimentation with 2nd generation wind tunnel model which will be capable of:
  - Boundary layer thickness measurement using rake
  - Pressure using Pitot tubes
  - Shear stress using experimental sensors
  - Correlation with established flow physics relationships

Next Steps-LaRC Shear Flow Wind Tunnel

- Test section: 20” × 28”
- Potential for extensive calibration in high quality tunnel
- Splitter plate set-up enables generation of reproducible, equilibrium turbulent boundary layer in the test section
- Well known boundary layer thicknesses, skin friction values, etc.
  - At 10 m/s, *y+* (wall unit) = 40 mm, τ (skin friction) = 0.3 Pa
  - At 40 m/s, *y+* = 11 mm, τ = 2 Pa

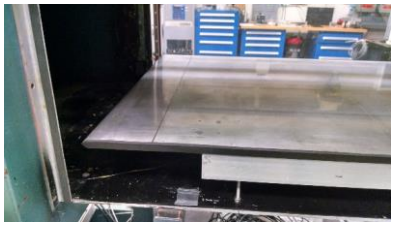

Elliptical Leading Edge and Trip Line

10” x 7” Insert in Test Section

Distribution/Dissemination

Invention Disclosures:

- Palmieri, Frank P.; Wohl, Christopher J.; Connell, John W.; Sheplak, Mark. Shear Stress Sensing using Elastomer Micropillar Arrays, *LAR-18336*, 2013, provisional patent application filed.

Publications:

- Wohl, Christopher J.; Palmieri, Frank L.; Hopkins, John W.; Jackson, Allen M.; Cisotto, Alexxandra A.; Lin, Yi; Connell, John W. "Flexible Micropost Arrays for Shear Stress Measurement" *NASA Technical Publication*, 2015, accepted.

Presentations:

- Cisotto, Alexxandra; Palmieri, Frank L.; Lin, Yi; Saini, Aditya; Kim, Jinwook; Kim, Taeyang; Connell, John W.; Zhu, Yong; Gopalarathnam, Ashok; Jiang, Xiaoning; Wohl, Christopher J.; Shear Stress Sensing with Elastic Microfence Structures, *AIAA Aviation 2015*, Dallas, TX, June 22-26, **2015**.
- Wohl, Christopher J.; Palmieri, Frank L.; Lin, Yi; Jackson, Allen M.; Cisotto, Alexxandra A.; Sheplak, Mark; Connell, John W. Shear Stress Sensing using Elastomer Micropillar Arrays. *246th American Chemical Society National Meeting*, Indianapolis, IN, *September 8-12*, **2013**.

Phase II Accomplishments

- Successfully initiated a cooperative agreement with NCSU Department of Mechanical and Aerospace Engineering
- Demonstrated instrumentation capable of detecting microfence deflection
- Demonstrated microfence deflection in wind tunnel as well as dependence of deflection on wind speed
- Demonstrated sensitivity to deflection of two other sensor designs using capacitance variation between two electrodes and piezoelectric response
- Through interaction with the Flow Physics and Control Branch (LaRC) designed and initiated fabrication of a wind tunnel model dedicated to shear stress measurements in subsonic turbulent flow
- Identified funding opportunities and will continue to seek funding for this research

3rd Party Information

- Slides containing 3rd party information that should be permissible due to the Fair Use act points:
  - Purpose of use-transformative for scholarship purposes
  - Nature of work-published, dissemination beneficial to the public
    - Slide 4: Insect website- http://cronodon.com/BioTech/insect_mechanoreceptors.html; Fish cilia- Soft Matter, 2009, 5, 292-295.
    - Slide 5: Ioppoli-44th AIAA Aerospace Sciences Meeting, Paper 649, Reno, NV, January 9-12, 2006.; Sheplak Image-Progress in Aerospace Sciences, 2002, 38, 515-570.
    - Slide 8: Jaganathara, R. K. et. Al., IEEE, 2009.
    - Slide 9: Int. J. Heat Fluid Flow 2008, 29, 830; Meas. Sci. Technol. 2006, 17, 2689; Meas. Sci. Technol. 2008, 19, 015403.